First Investigation on a Two-stage CERN PSB Collimation System

Penelope Jackson

Lady Margaret Hall

Thesis submitted in fulfilment of the requirements for the degree of Master of Science by Research at the University of Oxford

Trinity Term 2011

First Investigation on a Two-stage CERN PSB Collimation System

Penelope Jackson

Lady Margaret Hall

Trinity Term 2011

Abstract

This thesis investigates the feasibility of a two-stage collimator for the PSB (Proton Synchrotron Booster) at CERN. Simulations of several shapes, sizes and materials were run and the indications from this study are that due to heating concerns either diamond is required for the first stage or a fast kicker would need to be installed to prevent damage in the event of beam loss. Aluminium is also possible with some compromise on performance. The final design would be subject to further simulations on nuclear scattering effects and requires the exact tune to be known; a parameter not yet decided.

Acknowledgements

Thanks to my official supervisors Ken Peach in Oxford and Christian Carli at CERN for all their help, and my not quite official supervisor Emmanuel Tsesmelis at CERN who was incredibly helpful despite all his other obligations.

My office mates Myriam Newman at CERN and Suzie Sheehy in Oxford were always very helpful whenever I needed it, and great company.

Todd Huffman, my college advisor was excellent as was Rev'd Allan Doig, the college Tutor for Graduates. Both always showed genuine interest for my academic well-being in what could have been very token roles.

Thanks to all other technicians and academics who answered questions that couldn't be resolved by anyone previously mentioned!

Contents

List of Figures

List of Tables

1. Introduction to the LHC Accelerator Upgrade

Particle accelerators and their detectors are the tools of high-energy physics, and to push forward the frontiers of the field new accelerators are always needed. The main ways of making new discoveries are higher luminosity to see more rare events and higher energy to create particles which have never been observed before, the most famous example being the Higgs Boson. CERN has the highest energy accelerator ever built; the Large Hadron Collider (LHC) near Geneva in Switzerland, currently colliding protons at a centre of mass energy of 7 TeV (3.5 TeV per beam). [1]

To reach such a high energy, particles need to be accelerated several times by a series of larger and larger machines (see figure 1). They start in the Duoplasmatron proton source and are first accelerated by a linear accelerator (LINAC 2) to 50 MeV. They then go on to the Proton Synchrotron Booster (PSB or PS Booster, just "Booster" in the diagram below) up to 1.4 GeV, followed by the Proton Synchroton (PS) to 25 GeV, the Super Proton Synchroton (SPS) to 450 GeV and finally the LHC itself, which will eventually run at a centre of mass energy of 14 TeV (7 TeV per beam). [2][3]

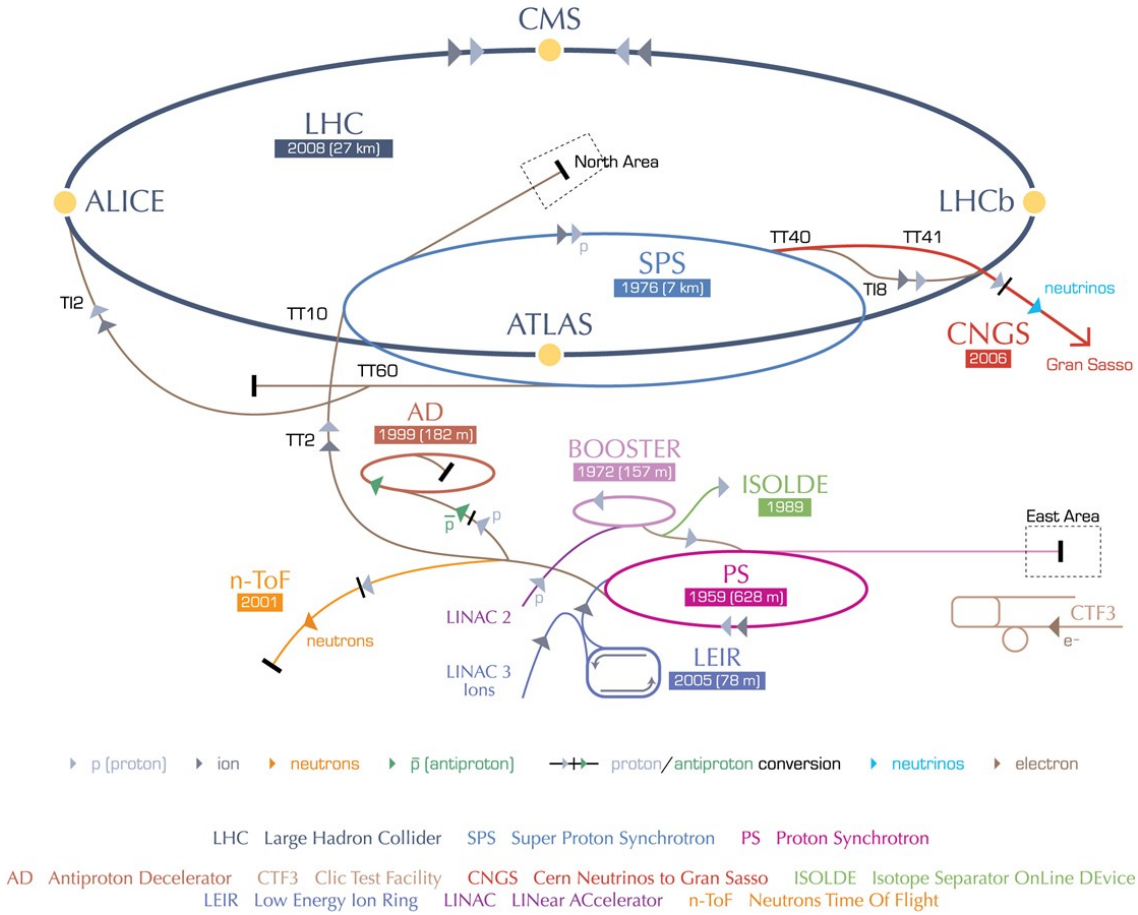

Figure 1: *The current CERN accelerator complex. [4]*

The CERN accelerator complex is ageing and is not optimised for current and future projects. The oldest machine, the PS started operations in 1959 so is now over 50 years old. There is a proposal to replace LINAC2 with LINAC4 accelerating H^- ions to 160MeV, the PSB with the Superconducting Proton Linac (SPL, initially the Low Power SPL, LP-SPL), and the Proton Synchrotron with the PS2. The LP-SPL will be 430m long and able to produce 10^{14} protons for injection into the PS2 at 4 GeV. The full SPL will be 500m long and accelerate 1.1×10^{14} protons to 5 GeV, or 2×10^{14} to 2.5 GeV. [5] Both give an 80mA current, the LP-SPL for 0.4ms with a 2Hz repetition rate and the full SPL for 1.2ms with a 50Hz repetition rate. [6]

LINAC4 was intended eventually to be the low energy, normal conducting section of the SPL after a few years of LINAC4 standing alone and feeding into the PSB. This now looks more

likely to be a long term solution, with upgrades to the PSB and SPS and no replacement for the PS, the oldest accelerator still in operation at CERN. This thesis is about the LINAC4 injecting into the PSB scenario and one change which might have to be made to the PSB as a consequence. Figure 2 shows the proposed layout of the LINAC4/SPL and PS2 complex.

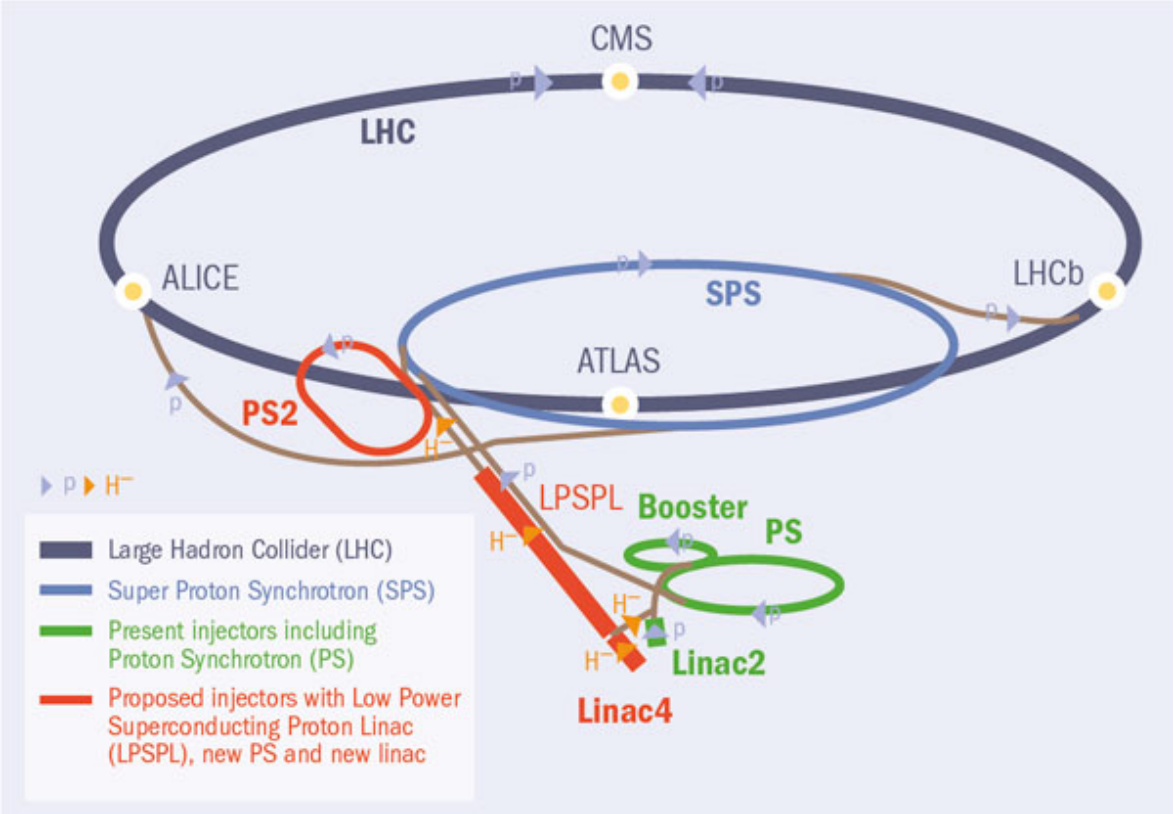

Figure 2: *The proposed new accelerators, the SPL and PS2, and how they fit in with existing machines. [7]*

The PSB is an unusual design consisting of 4 parallel rings stacked on top of each other, this is so the PSB extracted beam can fill the PS, a single ring of 4 times the circumference. However, it is now usually run with only one bunch per ring which requires two lots of protons from the PSB to fill the PS. This is done in order to minimize tune shift (unwanted spread of particle momenta). [8] Protons are injected into the PSB by multiturn injection. A 6m long section of the orbit is displaced out towards a septum magnet and four kicker magnets move it slightly

inwards each turn. This stacks beam in horizontal phase space over several turns before putting the beam onto its normal closed orbit. For lower intensity it can also be done in one turn. [9] It can take up to 1.2×10^{13} particles per bunch and accelerates them in 530ms. [10] [11]

Figure 3: *The PSB. Most of the beam-pipes are encased in magnets and RF cavities, but the four pipes can be seen towards the left of the photo.*

The luminosity and intensity of the CERN PSB are currently limited by direct space charge (the like charges of the protons repelling each other) at injection energy, which defocuses the beam. The main motivation for a PSB luminosity increase is to allow higher luminosity and faster filling of the LHC, but other experiments such as ISOLDE (On-Line Isotope Mass Separator, produces radioactive beams, more information in [12]) will also benefit from higher luminosity of the PSB. LINAC4 is proposed to allow higher intensity in the PSB by injecting at a higher energy (160 MeV as opposed to the current 50 MeV), relativistically reducing space charge effects. LINAC4 will also accelerate H^- ions (LINAC2 accelerates protons) which allows injection into the PSB via charge exchange. This happens in an injection chicane (figure 4),

combining the injected and circulating beam using a dipole magnet, involving fewer injection losses than the current method.

Immediately after the magnet is a stripping foil to remove the electrons from the H^- ions to convert it into a proton beam. Two further dipole magnets deflect the beam out of the main orbit and back in, allowing room for a dump to catch any particles that were not fully stripped.

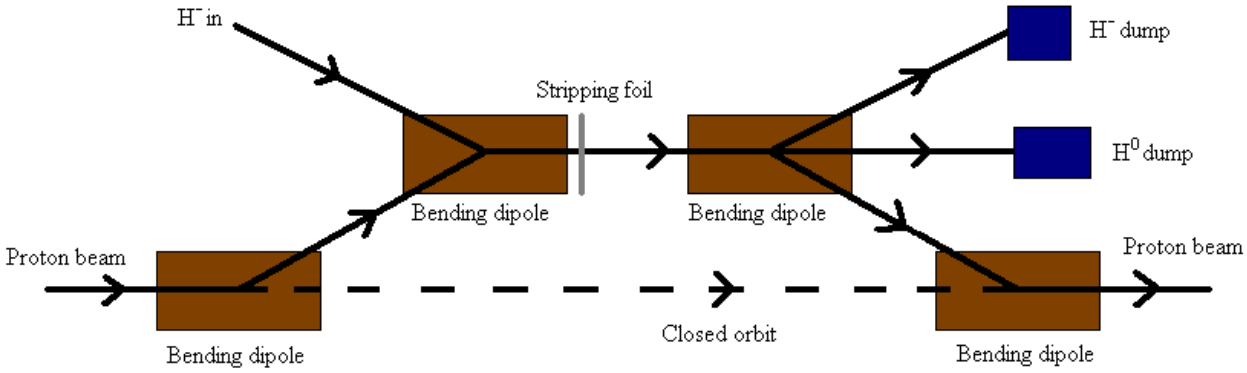

Figure 4: *How a charge exchange injection works. The closed orbit is the path the beam takes when the bending diploes in the injection system are off.*

The higher extraction energy of LINAC4 in principle allows 1.6 times as many protons to be injected into the PSB, 1.5× being required for the ultimate LHC luminosity. [13] LINAC4 also requires a new H^- source as the current source produces protons. [2] The LINAC4 source will have a higher repetition rate of 2Hz compared to the current 0.83Hz. [14][15] This means that the PSB can take a beam from the Linac every 0.5s instead of the current 1.2s before acceleration and passing on to the PS, and this time saving means the LHC can be filled faster.

The SPL has long-term aims for projects other than the LHC. For the LHC luminosity upgrade only the low power SPL (LP-SPL) is required. It is foreseen that long term future projects such as a neutrino factory or muon collider could benefit from the completed SPL. The SPL top

energy is up to 4 GeV compared to the PSB's 1.4 GeV, much better for injection into the PS2 which would have a top energy of 50 GeV compared to 25 GeV at the PS (see figure 2). [16]

The fully upgraded LHC ($10^{35}cm^{-2}s^{-1}$) [17] requires a significant upgrade to the injection chain, such as the SPL and PS2 described earlier or upgrading the PSB to 2 GeV. [18] The current injector chain has a theoretical maximum LHC luminosity of 10^{34} $cm^{-2}s^{-1}$; LINAC4 and the LHC machine changes described later should improve this by a factor of two or three. [19]

The SPS was not previously a priority for the luminosity upgrade but has been identified as a significant bottleneck due to its impedance (analogous to resistance if you treat the beam as a current) being higher than that of the LHC. Ways to reduce this are still being investigated, but it has been identified that the SPS could benefit from an anti-electron cloud coating. [7][20]

The LHC machine itself is being upgraded at the interaction regions for the higher luminosity. The inner focusing triplets will be replaced, crab cavities to rotate bunches may be installed (the "early-separation" (ES) scenario), or there could be more intense bunches with a larger crossing angle ("large Piwinski angle" (LPA) scenario) [17] and some of the detectors will be upgraded to cope with the increased number of collisions. Crab cavities are RF cavities which rotate the bunches just before the interaction point in order to compensate for the crossing angle (see figure 5).

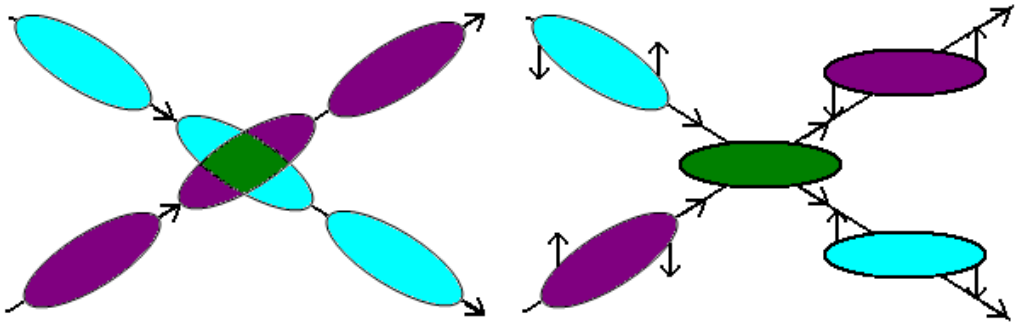

Figure 5: *How crab cavities increase luminosity. Without the crab cavities a large proportion of the bunches overlap when they collide, but with the crab cavities the bunches can be rotated until they fully overlap. They are then rotated back to along the beam direction after collision. [21]*

Another possible future plan is to upgrade the energy of the LHC to 28 or even 33 TeV [22] in the 2030s. This project is called the DLHC (Double energy LHC) or HE-LHC (High Energy LHC) and would require all magnets to be replaced in the LHC and SPS (to enable an upgrade to 1.3 TeV). This would require a very strong physics justification as it would effectively be two new large accelerators. Modifying the LHC to collide electrons and protons has also been suggested. [22]

2. Collimation and Theory

2.1 Collimation

After injection into the PSB, the higher energy beam from LINAC4 will be smaller than a beam with the same number of protons at LINAC2 energy, but will have more protons. The total number of lost particles from the edge of the beam is expected to decrease, but because they will be at higher energy, the protons hitting the beam-pipe will cause more debris and more machine activation (radioactivity) per proton than at lower energies, and possibly a higher level of activation than is acceptable in the machine.

The solution proposed in this thesis is a two-stage collimation system (diagram in figure 6) to remove protons in a controlled manner. This is an initial feasibility study on whether such collimation could solve this problem and if so, which collimator designs are likely to work best.

The system consists of a first thin scraper which scrapes the beam and then a second (graphite) absorber block further out from the beam. [23] This absorber means the radiation is contained in one location which can have more restricted access than the rest of the machine, or even be replaced if it gets too "hot" and will exceed safe radiation levels for people working in the tunnel if left any longer. The scraper should only deflect particles that are far enough out to be in an undesirable position and either deflect them outwards towards the absorber (but not necessarily straight in) or away but on a changed trajectory with a deflection and energy loss which should result in meeting the scraper again on a later turn. Particles are expected to start near the centre of the bunch and diffuse outwards so it is not expected that there will be many particles initially hitting the scraper a long way out, and very few that were already on a trajectory to hit the absorber are likely to be deflected away by the scraper. The particles removed are going to be mainly those with large betatron oscillation amplitudes as these make

up the majority of the particles on the outer edges of the beam, along with those with a large momentum offset.

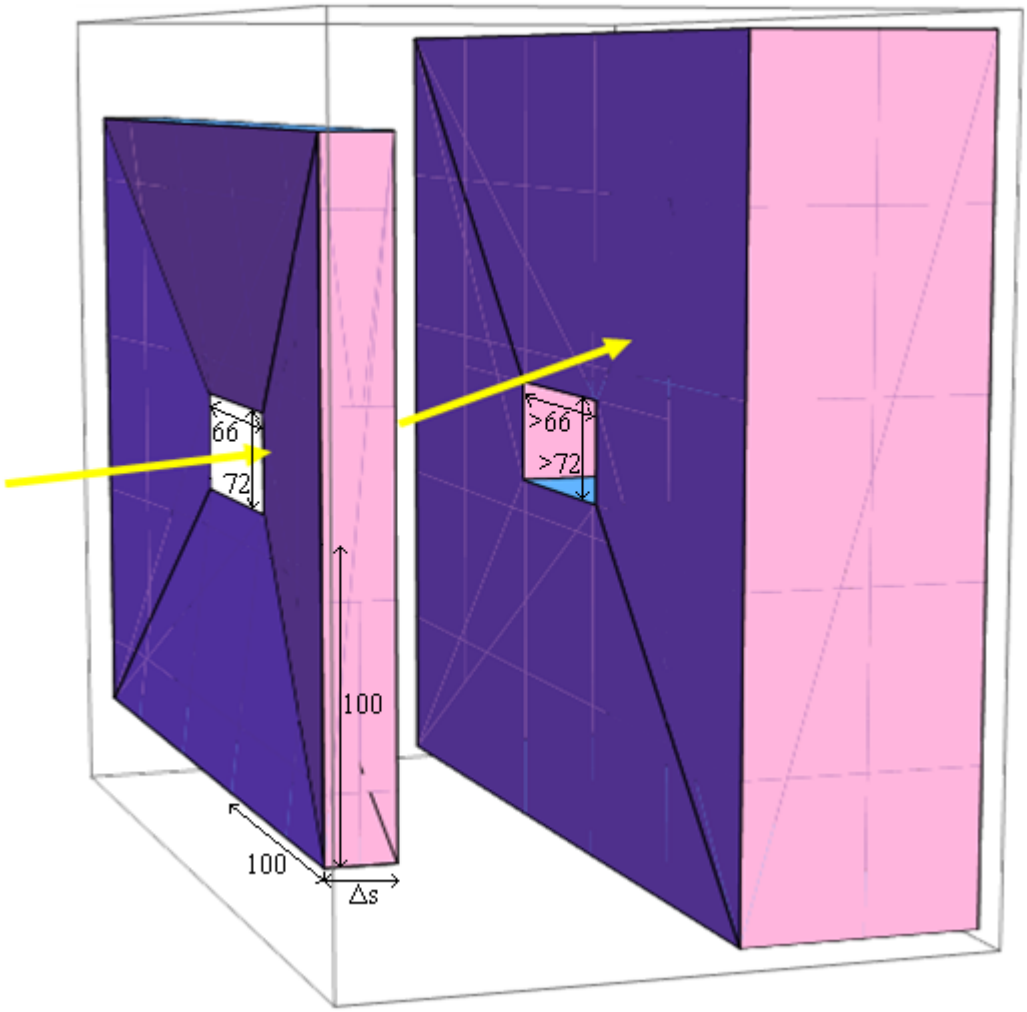

Figure 6: *The full collimator. The beam shown by the arrow goes from left to right, and should be deflected by the scraper. Immediately or after more turns it should be absorbed on the face of the absorber. All distances are in mm.*

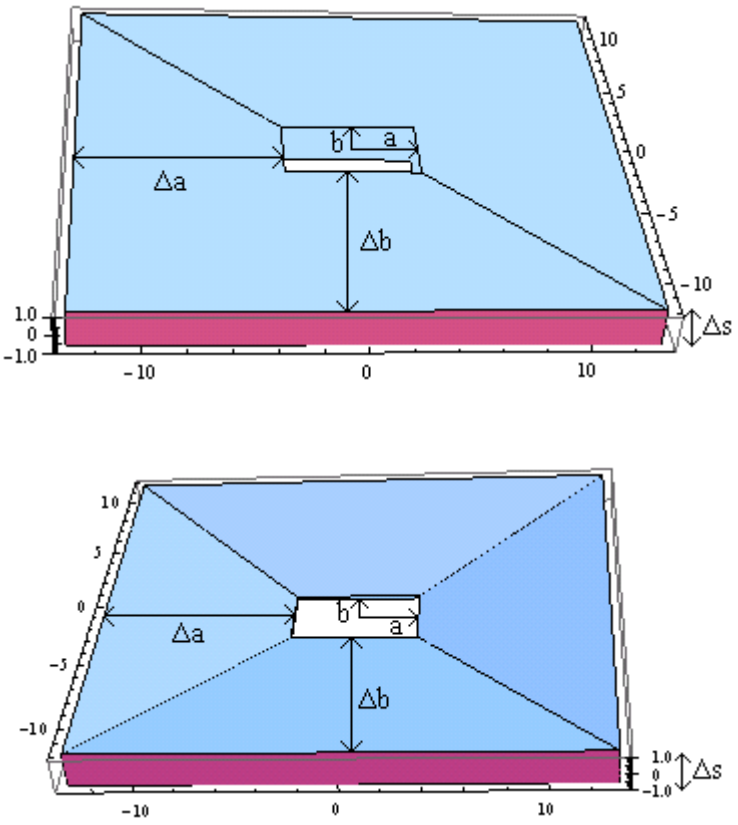

Figure 7: *A diagram of the two proposed scraper shapes. The one above has a constant thickness, the one below a wedge much narrower at the centre than the outside, not to scale. Axes (indicating aperture size) are in mm.*

The first stage of the collimator (the scraper) has a horizontal aperture extending to ±a and vertical aperture to ±b and the thickness depends on the cross-sectional shape as in figure 7 above. For a rectangular scraper it is denoted Δs, for a wedge shaped one Δs denotes the thickness at a distance ±Δa and ±Δb from the inner edge of the scraper (in all cases here, Δa = Δb = 10cm). This creates a known opening angle, and the width for a given hit (here for an x offset) is given by

$$ds = \frac{\Delta s}{\Delta a}(|x| - a) \tag{1}$$

where ds is the distance along the beamline.

The scraper has an aperture of 66 × 72 mm^2 and the absorber block aperture has to be bigger than this; the behaviour of the system changes depending on how much bigger the absorber block aperture is. The material of the scraper, shape (rectangular cross-section or wedge) and thickness/opening angle also make a difference.

2.2 Simulation and Theory

The PSB is modelled by two transfer matrices described later in this section, one taking particles from the scraper (denoted point 1) to the absorber (point 2), and the other from the absorber back to the scraper (if the particle has not been removed). No separate matrix is used for the absorber, since it is presumed to be relatively short and to have no significant effect on the machine parameters. The absorber would probably be modelled as a drift length, which is how it is implicitly indicated in the transfer matrix. On hitting the scraper the particle is scattered and loses momentum, changing its orbit. If this new trajectory sends it into the absorber or the beam-pipe (outside machine acceptance), the simulation is stopped, otherwise it takes another turn and may be scattered again. This is repeated for many particles, usually 10,000, reducing the uncertainty to about 1%. The fraction that hit the absorber (compared to those lost by being outside the machine acceptance), the fraction of the absorbed particles that did at least one more turn after hitting the scraper and the RMS scattering angle are all recorded.

The particle has an initial vector *r* consisting of the x position, horizontal angle x', y position, vertical angle y' and momentum offset as a fraction of total momentum $\frac{\Delta p}{p}$, which starts as

$$r = \begin{bmatrix} x_{in} \\ 0 \\ y_{in} \\ 0 \\ \frac{\Delta p}{p} \end{bmatrix} \tag{2}$$

Only the $\frac{\Delta p}{p}$ in the x direction is taken into account as the effect on the radius of the particle's orbit is the only effect being considered here. In both planes it affects how the particle travels through focusing magnets, changing the tune.

A matrix of sine-like (S(s)) and cosine-like (C(s)) particle trajectories and their derivatives has to be constructed to map the particle's motion from point *i* to point *j*. We construct equation 4 given that at the starting point s_0 (where s is the distance), $S(s_0) = 0$, $S'(s_0) = 1$, $C(s_0) = 0$ and $C'(s_0) = 0$ and Hill's Equation (equation 3) because the trajectory is real. For the full derivation see [24] pp. 38, 56 and 62-64. Hill's equation is roughly simple harmonic motion:

$$y(s) = a\sqrt{\beta(s)}\cos(\Phi(s) - \delta) \tag{3}$$

where *a* is a constant, *β(s)* is the local beta function (bean envelope) *Φ* is the phase and δ is a small difference. We can now construct the matrix:

$$\begin{pmatrix} C(s) & S(s) \\ C'(s) & S'(s) \end{pmatrix} = m_{ij} = \begin{pmatrix} \sqrt{\frac{\beta_j}{\beta_i}}(\cos\Delta\Phi + \alpha_i \sin\Delta\Phi) & \sqrt{\beta_i\beta_j}\sin\Delta\Phi \\ -\frac{1+\alpha_i\alpha_j}{\sqrt{\beta_i\beta_j}}\sin\Delta\Phi + \frac{\alpha_i-\alpha_j}{\sqrt{\beta_i\beta_j}}\cos\Delta\Phi & \sqrt{\frac{\beta_i}{\beta_j}}\cos\Delta\Phi - \alpha_j\sin\Delta\Phi \end{pmatrix} \tag{4}$$

where *i* and *j* are 1 and 2 or 2 and 1 respectively. For m_{12}, $\cos\Delta\Phi = \cos(\varphi_{21})$ where $\cos\ \varphi_{21} = 2\pi \times Q_h - (\mu_2 - \mu_1)$; for m_{21}, $\cos\Delta\Phi = \cos(\mu_2 - \mu_1)$. Q_h is the horizontal tune, an equivalent analysis applies to *y* (vertical tune). μ is the phase advance, β is the beam envelope due to the magnets in the lattice and $\alpha = \frac{-\beta\prime}{2}$. [25 pp 32, 36]

These matrices are then used to create two 5 × 5 matrices with particle motion in *x* and *y* (the *x* and *y* subscripted elements are the horizontal and vertical versions of equation 4):

$$M_{ij} = \begin{pmatrix} m_{ijx} & 0 & D \\ 0 & m_{ijy} & 0 \\ 0 & 0 & 1 \end{pmatrix} \tag{5}$$

D is the dispersion, a function describing the motion of an off-momentum particle. Both elements are 0 for vertical motion. [25 p65]

$$D = \begin{bmatrix} \widehat{D}x_{ij} \\ \widehat{D}'x_{ij} \end{bmatrix} = \begin{bmatrix} Dx_j \\ D'x_j \end{bmatrix} - [m_{ij}] \begin{bmatrix} Dx_i \\ D'x_i \end{bmatrix} \quad (6)$$

The particle is tracked around the ring by these matrices, M_{12} takes from point 1 (the scraper) to point 2 (the absorber block). For particles that make it past point 2, matrix M_{21} takes it back to the scraper. r is updated each turn by $[r] = [M_{12}][r]$ at point 1 and then $[r] = [M_{21}][r]$ at point 2. These 5 × 5 matrices have a transfer matrix like eq. 3 in the top left 4 elements for the x components and another one in the 3rd and 4th row and column for the y components. A further column is for the dispersion, which is the widening of the beam due to off-momentum particles having a slightly higher or lower bending radius which changes their closed orbit (the ideal path a particle would take around the machine through the centre of the magnets with no offset or oscillations) [25 pp.64 – 65]. The magnitude of its deviation from the orbit for on-momentum particles is just proportional to the momentum offset $\frac{\Delta p}{p}$.

If the particle hits the scraper, the r vector is updated by

$$[r] = [r] + \begin{bmatrix} 0 \\ x\ deflection \\ 0 \\ y\ deflection \\ \frac{1}{\beta^2}\frac{dE}{dx}\frac{\rho ds}{KE+m_p} \end{bmatrix} \quad (7)$$

The x and y deflections are scattering angles modelled here by random numbers with a Gaussian distribution, with mean 0 and variance θ_{rms}. KE is the kinetic energy, β is the relativistic β, m_p is the mass of the proton and ρ is the material's density. This is not an ideal model as the distribution of scattering angles is not quite Gaussian, but is a good enough approximation for

the purposes of this initial study. [26 p224] The last element comes from $\frac{\Delta p}{p} = \frac{1}{\beta^2}\frac{\Delta E}{E}$, ΔE is $\frac{dE}{dx} \times \rho$ and $E = KE + m_p$.

The formula for energy loss through a medium is the Bethe – Bloch equation [26 p231]:

$$-\frac{dE}{dx} = Kz^2\frac{Z}{A}\frac{1}{\beta^2}\left[\frac{1}{2}ln\frac{2m_ec^2\beta^2\gamma^2T_{max}}{I^2} - \beta^2 - \frac{\delta(\beta\gamma)}{2}\right] \quad (8)$$

I is the mean excitation energy and T_{max} is the maximum kinetic energy that a free electron can get in a single collision [26 p232]:

$$T_{max} = \frac{2m_ec^2\beta^2\gamma^2}{1+2\gamma\frac{m_e}{M}+\left(\frac{m_e}{M}\right)^2} \quad (9)$$

Ignoring $\frac{\delta(\beta\gamma)}{2}$ as it is small at these energies and setting $Z = 1$ (incident particles are protons) this combines to:

$$-\frac{dE}{dx} = \frac{K}{A}\frac{Z}{\beta^2}\left[ln\frac{2m_ec^2\beta^2\gamma^2}{I} - \frac{1}{2}ln\left(1 + 2\gamma\frac{m_e}{M} + \left(\frac{m_e}{M}\right)^2\right) - \beta^2\right] \quad (10)$$

β and γ are the relativistic β and γ ($\beta = 0.52$, $\gamma = 1.17$ at injection), $K/A = 0.307075$ MeV g^{-1} cm^2, Z is the atomic number of the material, M is the mass of the incident particle (proton), $m_ec^2 = 0.511$ MeV (mass of electron), $\frac{m_e}{M} = \frac{1}{1836}$. The particle also scatters randomly when it travels through the scraper, with an angle given by [26 p236]:

$$\theta_{rms} = \frac{13.6MeV}{\beta cp} \times \sqrt{\frac{ds}{X_0}} \times \left(1 + 0.038 \times ln\left(\frac{ds}{X_0}\right)\right) \quad (11)$$

where c is the speed of light, p is the momentum of the incident particle, ds is the distance traversed through the material and X_0 is the radiation length. This formula starts to break down at distances less than $10^{-3}X_0$. [26 p236] Depending on the scraper shape, when $|x| > a$, ds is either just Δs for a rectangular cross-section or for a wedge shaped scraper eq. 1 is corrected to:

$$ds = 10^{-4}X_0 + Max\left(\frac{\Delta s}{\Delta a}(|x| - a), \frac{\Delta s}{\Delta b}(|y| - b)\right) \quad (12)$$

10^{-4} rather than 10^{-3} is used because a small inaccuracy is preferable to disregarding any scattering at small distances, the scattering angles for these small distances still shrink in a sensible way as distances get smaller rather than starting to produce large negatives as will happen due to the *ln* term if distances much shorter than $10^{-4}X_0$ are used. An alternative solution would be not to add $10^{-4}X_0$ but to have the scraper not registered as being hit until it reaches this thickness; having this makes the aperture artificially large for very thin wedge scrapers as they are thinner than that for distance from the aperture slightly too large to ignore.

To pass point 2 (the absorber), the code first calculates if the particle hits the absorber block simply by checking if the scatter and energy loss from the scraper causes its *x* or *y* co-ordinate to be greater than the aperture of the absorber. If not, it could get lost in the machine by hitting the beam-pipe. This is to be avoided as much as possible because it makes the beam-pipe radioactive. To check if it hits the beam-pipe, equations 13 and 14 are used to see if its oscillations take it beyond the edge of the vacuum chamber in a typical section of beam-pipe (outside the acceptance). α_i and β_i here are the Twiss/Courant & Snyder parameters (note: not the relativistic β in eqs. 8 - 10).

$$\frac{\left(1+(\alpha_{2y})^2\right)y^2}{\beta_{2y}} + 2\alpha_{2y}yy' + \beta_{2y}(y')^2 > A_y \quad (13)$$

$$\sqrt{\frac{(1+(\alpha_2)^2)x^2}{\beta_2}\left(x - Dx\frac{\Delta p}{p}\right)^2 + 2\alpha_2\left(x - Dx\frac{\Delta p}{p}\right)\left(x' - Dx'\frac{\Delta p}{p}\right) + \beta_2\left(x' - Dx'\frac{\Delta p}{p}\right)^2} > \sqrt{A_x} - \left|\frac{\Delta p}{p}\right|\frac{D_s}{\sqrt{\beta_2}} \quad (14)$$

where A_x (A_y) is the aperture of the beam pipe in the horizontal (vertical) direction, x and y are the horizontal and vertical positions on reaching the absorber and x' and y' are the angles from the closed orbit they make.

3. Experimental Method

In this section the different parts of the study are discussed in separate subsections. Some were stand-alone studies; some had results which affected later sections. The results and conclusions from each are discussed in later chapters, which follow a similar format.

3.1 160 MeV Simulations

Since the beam gets smaller as energy increases, the largest beam and hence most losses will occur at the injection energy. A newly injected beam may also contain particularly off-momentum particles which should be removed as fast as possible. Therefore this proposed collimator is designed to work at injection and all performance considerations are for 160 MeV.

Using the calculations in the previous chapter, a *Mathematica* [27] programme (see Appendix 1 for the code) tracked simulated particles around the accelerator and determined if and how they were removed. This was run at the injection energy of 160 MeV when the beam would be at its widest and most of the collimation would happen. Ideally they should all be caught by the absorber, but in practice this does not happen. A parameter here called the efficiency is defined as:

$$Efficiency = \frac{N(Abs)}{N(Abs) + N(x) + N(y)} \tag{15}$$

where *N(Abs)* is the number which hit the absorber, and *N(x)* and *N(y)* are the number of particles outside the horizontal and vertical acceptance. Since they are dealt with separately, the beampipe is modelled as rectangular. It is actually oval but this would require the horizontal and vertical acceptances to be dealt with at the same time which is a lot more complicated and not necessary for a study as basic as this.

Another important parameter "multi turns" is the fraction of particles that made multiple turns, i.e. did not hit the absorber during the first turn after hitting the scraper. All simulations were done with a test particle with initial conditions to make it hit the scraper on a known turn number.

Higher multi turns and therefore thinner scrapers are better because of something known as the impact parameter *d* (see figure 8). If it is very small or zero, the particle may hit the absorber but bounce off and possibly be scattered outside the acceptance. Ideally the stray particle should be almost parallel to the beamline and hit the absorber at right angles to the facing edge, not at an angle and graze a face of the absorber orientated parallel to the beam. The latter is likely to result in the particle being removed by a single large scatter sending it directly into the absorber. As many multiple hits as possible on the scraper theoretically makes the system better, but also makes heat damage worse.

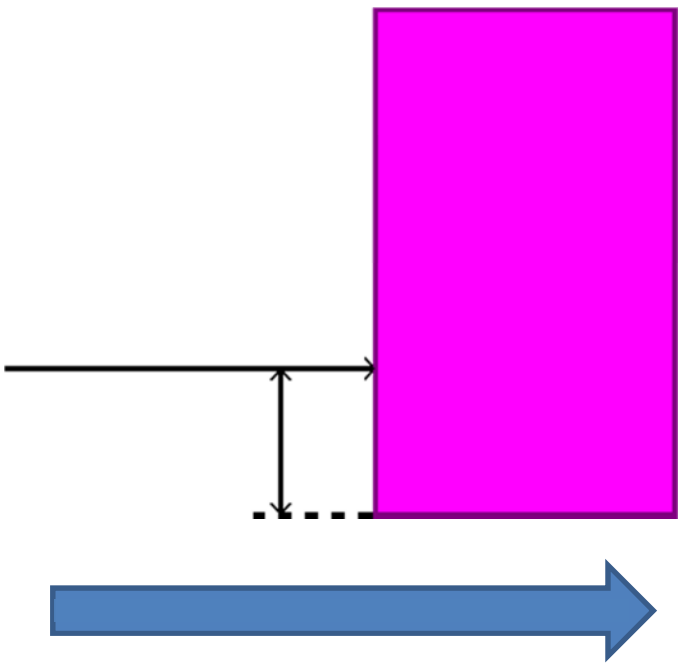

Figure 8: *Diagram to explain impact parameter* d*, the perpendicular distance from the aperture. The pink rectangle is a cross-section through the top part of the absorber, the blue arrow is the ideal beam position. The horizontal black arrow is the ideal path of a stray particle, into the absorber with a large* d*. This is most likely to happen after several scatters by the scraper.*

A scraper efficiency and multi turns fraction both of 90% were aimed for. The PSB currently suffers some losses and it has yet to be seriously damaged by activation from standard use, the configuration with LINAC4 would mean these losses occur at higher energy and do more damage. Taking out around 80% of the expected losses should reduce the activation to below the current levels, extending the lifetime of the machine. Generally the horizontal phase space has better performance than the vertical, and a scraper efficiency of around 80% is tolerated for vertical phase space. From flat scrapers for the first four materials, an acceptable performance occurs when

$$\frac{\Delta s Z}{X_0} = 0.025 \text{ to } 0.054 \tag{16}$$

where Δs is the thickness, X_0 is the radiation length and Z is the atomic number. This is an empirical result found from the first few materials to get a rough idea of where to look for suitable thicknesses for later ones, not calculated from any theory. There was little correlation between the value of Z and where in this range the limit of suitable scraper performance was. The simulation is run to calculate the efficiency and multi turns (with thicknesses in the range of equation 16) and so find the maximum suitable thickness for a flat scraper.

An interesting modification to make to this was to correct for radiation length and nuclear charge by multiplying the thickness by the atomic number divided by the radiation length which should have made the graphs of efficiency and multi turns overlap for the different materials. This is included in the results in figures 17 – 21 in section 4.2.

3.2 1.4 GeV Simulations

The study was repeated using protons at the extraction energy of 1.4 GeV as while the number of losses is expected to be much smaller, the energy deposited per particle is much higher. The simulation had subtle changes made to allow for this; numbers which had previously been hard-coded were made variable to allow them to be adjusted to a different energy and the usual input parameters were changed to give a higher maximum number of turns (10^6, previously 200). This was done when it was clear that 1.4 GeV simulations involved significantly larger numbers of turns due to much smaller scattering angles; the previous threshold cut off many of the particles which were going to hit the absorber. This is probably because the slower diffusion means there is a strong dependence on distance travelled through at the tip of the wedge as the particles spend more of their time near the edge of the aperture. Particles would probably never spend 10^6 turns at top energy in the machine but this number was chosen to give good statistics on what happens to the particles as much less than this means it often takes more turns than the simulation allows for the particle to be removed.

The simulations were not repeated for the whole range of thicknesses, but just those selected as suitable from the 160 MeV studies (0.1mm tungsten, 0.7mm copper, 4mm aluminium and 10mm graphite wedges, 0.1mm aluminium and 0.2mm graphite flat).

3.3 Tune Variation

The PSB tune with LINAC4 has not yet been decided, so the effect of the tune being different from the one assumed in the initial simulations needs to be known as it could have a significant effect on performance.

The collimation was simulated as usual with vertical tunes over a range from 4.45 to 5.25, with increments of 0.01, using a tungsten wedge scraper of maximum thickness 1mm, an aluminium wedge of maximum thickness 4mm and a flat aluminium scraper of thickness 0.1mm. The same

parameters as in the main collimation study were used and recorded: efficiency (fraction of particles hitting the absorber), multi turns (fraction of particles making at least one full turn after hitting the scraper) and average number of hits on the scraper made by the particles in the simulation. 10,000 particles of the same initial properties were used as usual to get statistics to a significance of around 1%.

A 0.1mm flat tungsten scraper was also tried briefly but there appeared to be no change in behaviour with tune variation, the multi turn behaviour was very poor and the average number of hits on the scraper stayed around 1.

3.4 Heating

It is important to consider off-momentum particles depositing large amounts of energy in the scraper as there could be enough energy deposited to cause serious damage to it. This is likely to have an effect on which materials to use, possibly justifying ones which are more expensive or difficult to work with, which would not otherwise be first choice. If no suitable materials can withstand the maximum possible energy deposition a protection system needs to be implemented.

To get a first idea of how to solve the problem and to estimate roughly the size of the effect, a simple model with no conduction or radiation was used.

For all materials, simulations at 1.4 GeV calculated the average number of hits on the scraper per particle and indicated that 18 – 19% of turns hit the scraper. With a revolution time of 10^{-6}s the time for the particle to be lost can be calculated and thus the time taken for the scraper to reach its maximum temperature, or melting point if lower.

Given the number of hits and the material properties, the heat gain was calculated in another simple simulation.

The energy deposited per hit was calculated by

$$E = \frac{dE}{dx}\rho\Delta s \tag{17}$$

where $\frac{dE}{dx}$ is from the Bethe-Bloch equation, ρ is the density in g/cm^3 and Δs the scraper thickness in cm.

The temperature rise was then calculated by

$$\Delta T = \frac{E\ n_{hits}\ e\ n_{pcls}}{\rho\ A\ \Delta s\ C_v} \tag{18}$$

where E is the energy loss in eV as calculated in equation 17, n_{hits} is the average number of times each particle hits the scraper, e is the charge on the electron in Coulombs, n_{pcls} is the number of particles in the beam, A is the area in cm^2, Δs is the thickness in cm and C_v is the heat capacity in J/g K.

Lithium and boron are not practical scraper materials, but have been included in this study to explore behaviour at low atomic numbers.

Properties for each material were ascertained as inputs for *Mathematica* calculations; these are in table 1 below. [28][29][30][31][32][33][34][35][23]

Material	Specific heat C_v (J/g °C)	Conduc-tivity (J/cm °C s)	Atomic number	Radiation length (g/cm^2)	Density (g/cm^3)	Mean excitation energy (eV)	Thickness (mm)
Graphite	0.6904	0.238	6	42.70	2.210	79	0.2
Aluminium	0.8996	2.22	13	24.01	2.699	162	0.1
Copper	0.3849	3.93	29	12.86	8.960	311	0.02
Tungsten	0.1339	2.01	74	6.76	19.30	742	0.005
Beyrillium	1.824	1.82	4	65.19	1.848	58	0.8
Diamond	0.5104	23.2	6	42.70	3.52	79	0.2
Lithium	3.598		3	82.78	0.534	46.3	1.8mm
Boron	1.025		5	53.20	2.46	69.7	0.25mm

Table 1:*.Properties of the materials investigated. Conduction was not investigated for lithium or boron.*

Thickness was defined by the maximum acceptable flat (when possible) scraper at 160 MeV, given by multi turns × efficiency of around 80%. For Tungsten none of the thicknesses tried for flat scrapers was anywhere near that figure (all were far too thick with very poor performance) so instead the flat equivalent of the 0.1mm wedge was found. This was obtained from looking at the correlation between RMS scattering angles for flat and wedge scrapers, Tungsten wedges of a given maximum thickness had roughly the same RMS scattering angles of a flat scraper 1/20 the thickness of the wedge's maximum. The Bethe-Bloch energy loss given by equation 8 was used to find the energy loss per hit on the scraper and then multiplied by the density and thickness (which later cancels out).

The total energy deposited in the scraper was found by multiplying this by the average number of times each particle hit, the number of particles and converting from MeV to Joules. Average

numbers of hits were found with simulations of 10,000 particles at 160 MeV and 1.4 GeV using the code for scraper simulation. The number of hits is the only way the thickness makes a difference. The temperature change was found by:

$$\Delta T = \frac{Q}{mC_v} \tag{19}$$

where Q is the energy input (calculated as above), m is the mass and C_v is the constant volume specific heat, although for a solid rather than a gas constant volume is more or less a given. Since the mass is found from the volume × density and the volume involves the thickness, this cancels with the thickness to find the energy loss per hit.

The number of hits per particle was estimated from the model of the particle going around the machine as normal with the collimator. This is probably inaccurate because in addition to scattering, the change in central orbit will send the particles into the absorber more quickly. However, this should almost certainly overestimate the number of hits to lose a particle and slight overestimates are needed to ensure the system would be safe.

The other important quantity to estimate is the number of hits per unit area, requiring the number of particles in the beam, the beam size and distribution. There are 2×10^{13} particles per beam, and the beam size has been measured at extraction on a CNGS (CERN Neutrinos to Gran Sasso [36]) cycle to be σ_y = 2.28mm (see appendix 5) and 3 standard deviations taken to include most (>99%) of the particles. The beam with LINAC4 aims to be about the same size. The CNGS cycle was used because it is higher intensity than an LHC cycle so is better for worst case scenario calculations. This gives the vertical size of the area being hit. The horizontal size is assumed to be 3mm as due to the absorber aperture being 3mm larger than the scraper, so that very few particles will hit further out than 3mm. The distribution has been approximated to triangular as the maximum density of hits will then just be double the mean. This is modelled here by halving the area, giving an area of 0.1025cm^2 at 1.4 GeV, assuming a normalised

emittance (see below); the area will be 3.75× bigger at 160 MeV due to equation 20. The most useful beam size is that at extraction because the number of hits per particle before being scattered away at low energy is so low it is not of interest for calculating a worst case scenario.

The normalised emittance (ε_N) is a quantity which stays constant with the beam energy as the emittance changes during acceleration, and can be used to calculate the emittance at one energy given the emittance at another known energy. The normalised emittance $\varepsilon_N = \varepsilon\beta\gamma$ (where ε is the emittance and β and γ are the relativistic β and γ) stays constant if the only change in ε is directly due to the acceleration of the beam. Assuming the beam size σ stays the same relative to ε, knowing β and γ at injection and extraction, and σ at extraction (σ_1) we can find σ at injection (σ_2) by:

$$\sigma_2 = \frac{\beta_1\gamma_1\sigma_1}{\beta_2\gamma_2} \tag{20}$$

The low energy figures in the results section are not completely accurate because they use the beam size at extraction. However, since they are smaller and the actual beam size would only lower them further they have been included to demonstrate that the limitation is extraction energy.

Even without scattering, the beam could be lost due to the change in closed orbit. This could possibly be modelled by decreasing the energy each turn in the *Mathematica* simulation to compensate for the change in magnetic field. However, losses appear to be dominated by scattering rather than the movement of the beam over the scraper. Estimates of the total number of turns (not just hits) indicate in the region of 1000 turns (about 0.145 of the turns hit the scraper), with 5×10^{-7}s per turn and the central orbit moving at 2m/s this is only a movement of about 1mm. Diffusion from scattering is probably 3mm as this is the difference in size between the scraper and absorber half apertures, beyond this particles would hit the absorber.

3.5 Conduction

A simplified model of the beam hitting the scraper with heat conduction has been made in *Mathematica* (Appendix 3). The model treats the beam as a circle incident on a disc with the size doubled to compensate for the fact that the real beam hits an area adjacent to an edge, which would give it close to half the area to disperse over. The disc is split up into narrow rings with the central 100 rings having beam incident on them. Each ring has heat transfer for it calculated using the temperature of the adjacent rings, and if relevant, the power of the incident beam.

Rather than the total power of the beam, the power per unit area is used to simplify the calculation. To get the temperature, this is multiplied by the area of each ring, and the net heat in or out is calculated. This is then divided by the heat capacity and the mass.

The area of where the beam hits the scraper is calculated the same way as in Section 3.4. In order to take into account the beam being more intense in the middle a triangular distribution is assumed making the maximum intensity simply double the mean, making an effective area of 10.25mm^2. However, due to the geometry here being a beam incident on the centre of a disc when what is being simulated is an edge the area is doubled to 20.5mm^2. The area is taken to be in a circle for this approximation, an area of 20.5mm^2 gives a radius of 2.55mm, and is divided up into rings for the simulation. The innermost 100 rings are defined as being inside the beam makes the incremental radius of each ring-shaped element, Δr = 0.0255mm. The disc was extended well beyond the edge of the beam to an arbitrary 731 elements to give plenty of space for heat to conduct out of the edge of the beam.

The area of each annulus is $\pi\Delta r^2(n^2-(n-1)^2)$ where n is the ring element number, which simplifies to $\pi\Delta r^2(2n-1)$.

The equation for heat transfer in elements with beam taking into account heat in and out and the area connecting each element to its neighbour is:

$$T'_1 = T_1 + \frac{P/_A \Delta t}{\Delta s c_v \rho} - \frac{k\Delta t 2(T_2 - T_1)}{\Delta r^2 \rho c_v} \tag{21}$$

for element $n = 1$ (the central circular spot) and

$$T'_n = T_n + \frac{P/_A \Delta t}{\Delta s c_v \rho} - \frac{k\Delta t 2\big((n-1)(T_{n-1} - T_n) - n(T_n - T_{n+1})\big)}{\Delta r^2 \rho c_v (2n-1)} \tag{22}$$

for n = 2 onwards, where T_n is the temperature of the n^{th} element, t is time, k is conductivity, ρ is density, c_v is the specific heat, Δs the thickness and $P/_A$ is the power per unit area. The simulation was run with two arrays for temperature, T' updated as it ran through every element but getting T from an array not updated until the end of the time increment, when every ring element had its new temperature calculated. This is important because all spatial elements are supposed to be changed instantaneously in time, so the temperatures of adjacent elements must be from a temperature array which is fixed until the end of the time increment rather than the one updated during it. The two are set equal at the end of the time increment.

Without beam (for elements outside the beam or for the whole disc when the beam is off)

$$T'_n = T_n - \frac{k\Delta t 2\big((n-1)(T_{n-1} - T_n) - n(T_n - T_{n+1})\big)}{\Delta r^2 \rho c_v (2n-1)} \tag{23}$$

The beam x and y dimensions are calculated as σ_x = 2.28mm and σ_y = 3.29mm. Usually only σ_x was relevant, $3\sigma_x$ for horizontal size was taken and then multiplied by the 3mm aperture difference between the scraper and absorber for scattering in the vertical direction, giving an area of 20.5mm^2.

3.6 Radiation

While energy is being put into the scraper, its rising temperature means some is also being radiated and it was important to verify that this was not significant. To calculate it, a perfect blackbody was assumed. The Stefan-Boltzmann law gives [26 p4]:

$$\text{Power radiated (W)} = \sigma A T^4 \ \text{Js}^{-1} \tag{24}$$

where $\sigma = 5.6704 \times 10^{-8}$ W m^{-2} K^{-4}, A is the area in m^2 and T is the temperature in Kelvin. A was taken to be 2.05×10^{-5} m^2 and the temperature used is the melting point as this is the highest temperature of interest given the aim of this is to see whether radiation could prevent it melting.

The actual amount of radiation will be lower than this figure obtained from the temperature at the centre of the area hit by the beam. This is because the area has been scaled for the heating calculations which depend linearly on temperature whereas radiation scales with the fourth power of the temperature. This is sufficiently accurate unless this overestimated value turns out to be a large fraction of the input power.

The materials in this study are not perfect blackbodies, a more accurate formula is Power = $\varepsilon\sigma AT^4$. ε is the emissivity, a constant between 0 and 1 giving the fraction of radiation predicted by eq. 23 actually emitted, so the energy radiated is even less.

3.7 Variable Heat Capacities

Previously, all simulations have been done assuming that heat capacity stays constant with temperature, but this is not the case. For most materials it is close to its maximum value at room temperature and any changes at higher temperatures are negligible, but for carbon it is well below the maximum (see figures 9 and 10) and for copper it is about 25% lower. This means that diamond and graphite could take a lot more energy before melting/subliming than previous simulations have implied. Figure 9 shows how the diamond and graphite heat capacities change with temperature, figure 10 shows the smaller but significant effect for copper.

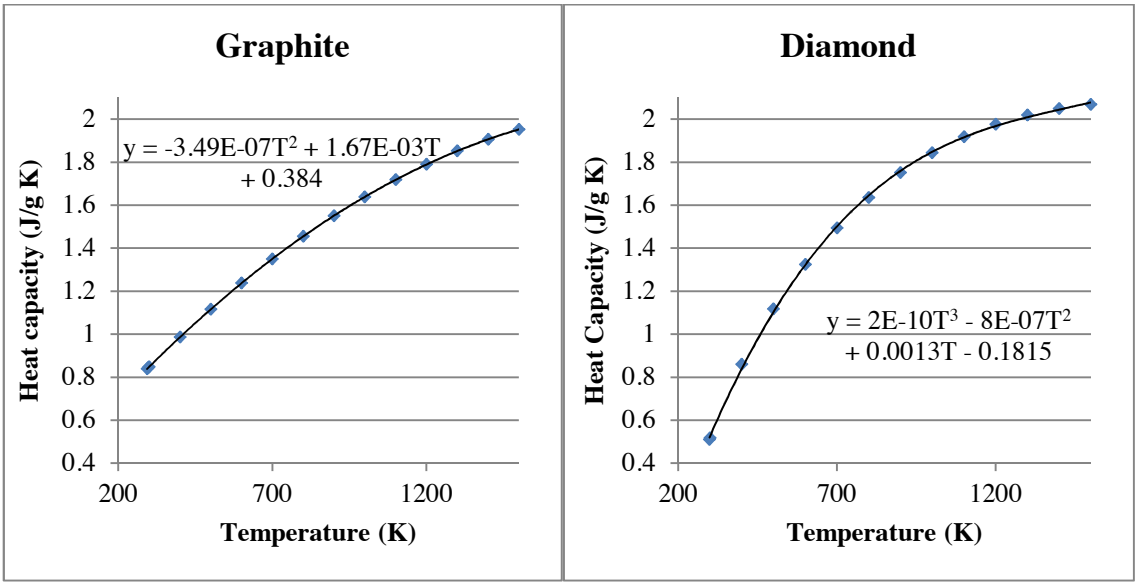

Figure 9: *How the heat capacities of graphite and diamond change with temperature.*

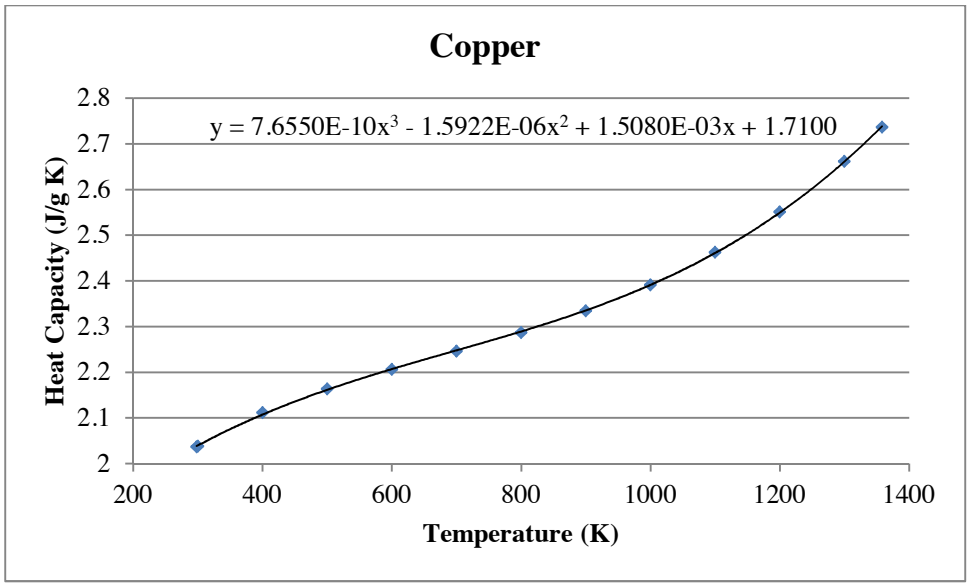

***Figure 10**: Change of heat capacity of copper with temperature.*

Simulations were made with no heat conduction or radiation as this has made no significant difference to the maximum temperature.

In [37] there is an approximate formula for how the heat capacity of graphite rises with temperature up to 200K. Reference [38] has tables with the heat capacity over a range of temperatures. These were plotted in Excel, and a best fit line was calculated with a cubic equation. The formula of this line was put into a *Mathematica* program (see Appendix 4) and depending on material, the Excel best fit for the equation from [37] was used to calculate the heat capacity for any heat. Since the temperatures involved went above where the extrapolated formula is valid, the heat capacity was assumed to stay constant above where the gradient went to zero.

This was done for graphite and diamond (which exhibits very similar behaviour) and copper. Copper has a much smaller change in heat capacity but large enough to be worth investigating (see figures 8 and 9). The graph stops at 1358K because this is the melting point of copper, how

the temperature rises above this is not of interest because the scraper needs to be solid even though the graph's shape implies the heat capacity could rise much further.

The *Mathematica* program was similar to the conduction case, which is a finite element analysis but in time as well as space. It was iterated for every hit up to the relevant average number of hits on the scraper, for each hit the heat capacity was calculated from the temperature after the previous hit and the heat deposited on that hit was calculated from this heat capacity.

3.8 Reducing the Number of Turns

Given that the optimal performance for many materials requires a scraper design which may be insufficiently robust to withstand beam loss, another approach was to investigate the highest possible performance scrapers which would withstand such a scenario. This was done by calculating the highest average number of hits on the scraper without melting it, then by trial and error finding a scraper thickness that could withstand a 1.4 GeV beam loss. It is possible to apply this new thickness to the number of turns established using the original thickness because the thickness makes no difference to the heating calculations. A thicker scraper means a longer distance along which to deposit energy but also a larger volume to hold it, and these exactly cancel out assuming insufficient energy loss to change dE/dx significantly.

The performance was then checked at 160 MeV as the scraper is mainly needed to remove stray particles at injection.

3.9 Nuclear Scattering

As well as the ionisation energy loss previously described using the Bethe-Bloch equation, beam particles can lose energy by scattering off nuclei in the material. To find how many such scattering events happen requires the number of scattering centres, the number of particles in the beam, and the cross section of each scattering centre (S_c).

First, the number of scattering centres (N_{S_c}, related to the volume) is calculated:

$$V = L \times area \tag{25}$$

where V is the effective volume and L is the effective length, in this case the thickness multiplied by the number of times travelled through.

$$Mass = \rho V \tag{26}$$

where ρ is the density.

$$N_{S_c} = N_{atoms} \times S_c/atom \tag{27}$$

$$N_{atoms} = V \times atoms/V \tag{28}$$

$$\frac{N_{atoms}}{V} = \frac{N_{atoms}}{mass} \times \frac{mass}{V} \tag{29}$$

$$\frac{Atoms}{mass} = \frac{N_A}{A} \tag{30}$$

where A is atomic mass and N_A is Avogadro's Number.

$$N_{atoms} = V \times \frac{N_A}{A} \times \rho \tag{31}$$

The number of scattering centres per atom is related to projected area, not just the number of constituent quarks. This is because unlike atomic nuclei in a solid, protons and neutrons in a nucleus can be treated as having no gaps in between.

$$Projected\ area = \pi r^2 \tag{32}$$

$$Volume = \frac{4}{3}\pi r^3 \tag{33}$$

Combining equations 32 and 33 gives:

$$r = \sqrt[3]{\frac{3V}{4\pi}} \tag{34}$$

$$Projected\ area = \pi\left(\frac{3V}{4\pi}\right)^{\frac{2}{3}} \tag{35}$$

$$S_c\ per\ atom = \pi\left(\frac{3A}{4\pi}\right)^{\frac{2}{3}} \tag{36}$$

Substituting equation 31 for the number of atoms and equation 36 back into equation 27:

$$N_{S_c} = \rho V \frac{N_A}{A}\pi\left(\frac{3A}{4\pi}\right)^{\frac{2}{3}} = \rho V N_A \left(\frac{3}{4}\right)^{\frac{2}{3}}\left(\frac{\pi}{A}\right)^{\frac{1}{3}} \tag{37}$$

Finally we get the number of events, N_{ev} by multiplying by the cross-section σ and the number of particles in the beam N_b:

$$N_{ev} = \sigma N_b N_{Sc} = \sigma N_b \rho V N_A \left(\frac{3}{4}\right)^{\frac{2}{3}}\left(\frac{\pi}{A}\right)^{\frac{1}{3}} \tag{38}$$

To find the value for the cross-section the momentum is needed, which can then be looked up in the tables in [39] and [40]. From the well-known equation:

$$E^2 = p^2 + m^2 \tag{39}$$

we can rearrange to get:

$$p^2 = (KE + m)^2 - m^2 \tag{40}$$

$$p = \sqrt{KE^2 + 2kem} \tag{41}$$

where *KE* is the kinetic energy and *m* is the mass of the particle (proton in this case). If this momentum is close enough to an entry in the table the cross section can be used. If not, assuming the relationship can be approximated as linear (which is probably valid for such small increments), it can be extrapolated from neighbouring values by

$$\frac{\sigma_x - \sigma_a}{\sigma_b - \sigma_a} = \frac{x - a}{b - a} \tag{42}$$

where x is the particle momentum, a and b are the nearest momenta below and above respectively, σ_x, σ_a and σ_b are their respective cross-sections. This can be rearranged to find σ_x:

$$\sigma_x = \left(\frac{x - a}{b - a}\right)(\sigma_b - \sigma_a) + \sigma_a \tag{43}$$

The energy loss per event is uncertain, see the discussion later, an upper bound of the total kinetic energy of the particle has been assumed.

4. Results

This section contains the results from all the subsections of chapter 3 and discussions of the implications of each result before moving onto the next. The conclusions are in the next chapter.

4.1 160 MeV Simulations

Scrapers of aluminium, copper, carbon (graphite here) and tungsten were investigated for different thicknesses along the beamline and for different sizes of the graphite absorber's aperture. For the rectangular cross-section (figures 11 – 13), thicknesses of 0.1 – 1mm were tried in 0.1mm increments, for the wedges (figure 14), 1-10mm in 1mm increments. In some wedge cases the efficiency was falling as the thickness approached zero and in most it was rising, so additional simulations were made for 0.02, 0.04, 0.06 and 0.08mm which showed it does rise at very small distances.

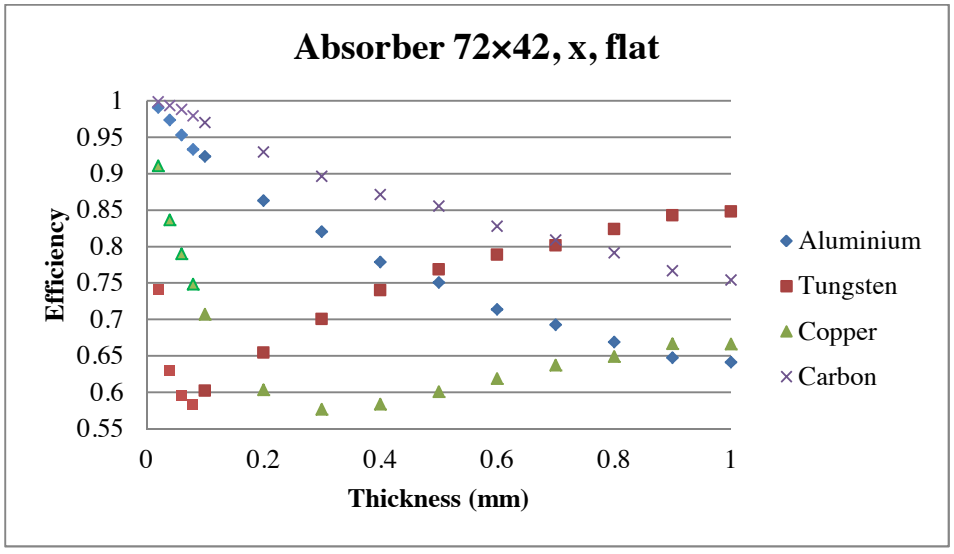

Figure 11: *Example of an efficiency graph comparing the different materials.72×42 is the absorber aperture and x refers to the particle being lost in horizontal phase space. Others were done for wedge collimators, vertical phase space and different absorber apertures.*

The effect in figures 11 and 14 (high efficiency when very thin, lower efficiency then rising again) which is visible in the graphs for materials with short radiation lengths is because there are three main ways to remove the particle. For very thin scrapers the particle is slowly dispersed outwards until it hits the absorber but is never outside the machine acceptance. For thick scrapers it gets a single kick straight into the absorber (which would in practice probably not be absorbed but that is not taken into account by these graphs alone). In between, neither of those happens as much because the most likely outcome is that particle gets a single kick which is too small to send it to the absorber, but it does not get a chance to be diffused outwards because the kick was big enough for it to be outside the acceptance and get lost in the machine. The efficiency graphs (figures 11, 14 and 15) are a combination of increasing efficiency with multiple scatters as the scraper gets thinner and apparent increasing efficiency from large single scatters as it gets thicker. The results here imply that a zero thickness scraper is best, this is due to the model used being an approximation which breaks down at very low thicknesses. Since scrapers this thin cannot be constructed, the approximation is still sufficient.

A scraper of aperture 66×36mm and an absorber of aperture 72×42mm are proposed. The simulations indicate an absorber x aperture up to ±37mm and y up to ±22 (74×44mm) work well for ideal shaped scrapers, because of uncertainties in the position of the beam these should be reduced by 1mm to ensure a margin of error. If it is very poorly positioned, the collimator could be adjusted, so that the alignment would be accurate to about 0.1mm. The machine tolerances can be as low as 0.01mm for some materials so this is much less of a problem. [41]

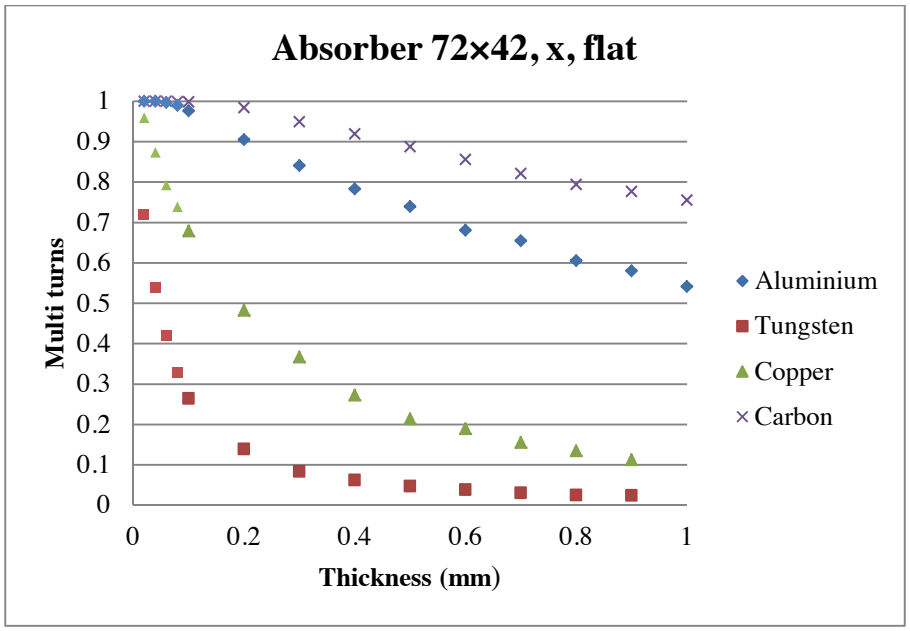

Figure 12: *Example of graph comparing multi-turn behaviour in the different materials for a given scraper design.*

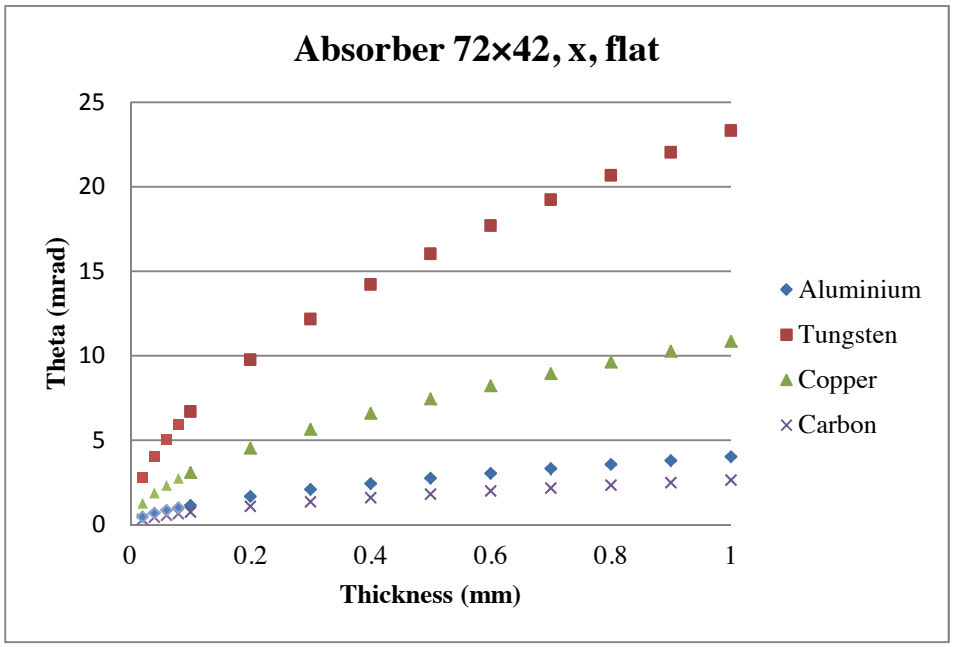

Figure 13: *Showing how the RMS scattering angle increases with thickness. It is dominated by the square root term.*

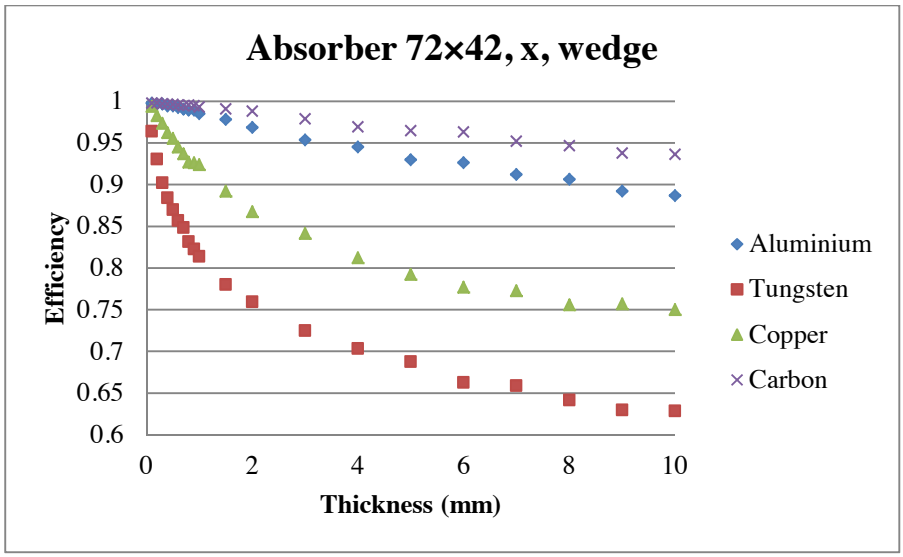

***Figure 14**: As figure 11, but with a wedge-shaped scraper.*

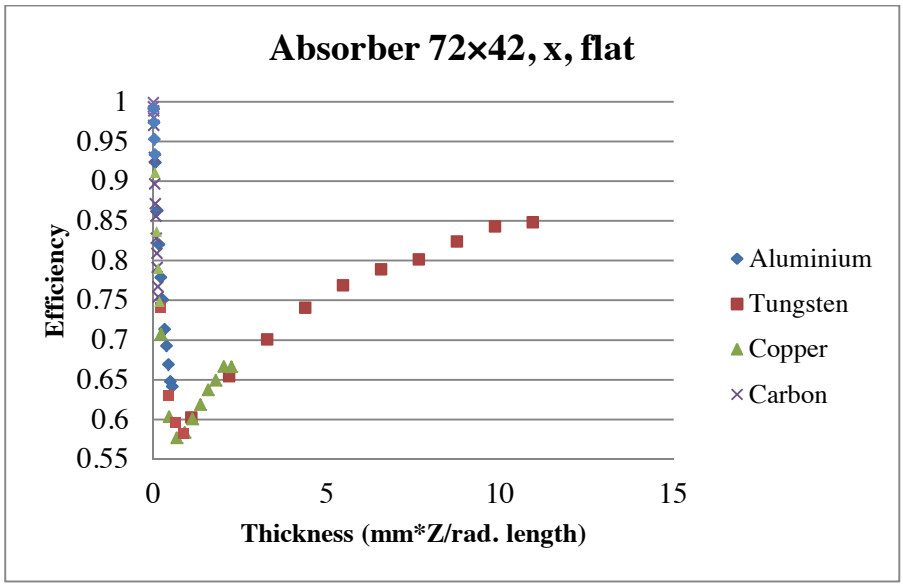

***Figure 15**: Comparing the efficiency graphs when the thickness is corrected for radiation lengths and atomic number.*

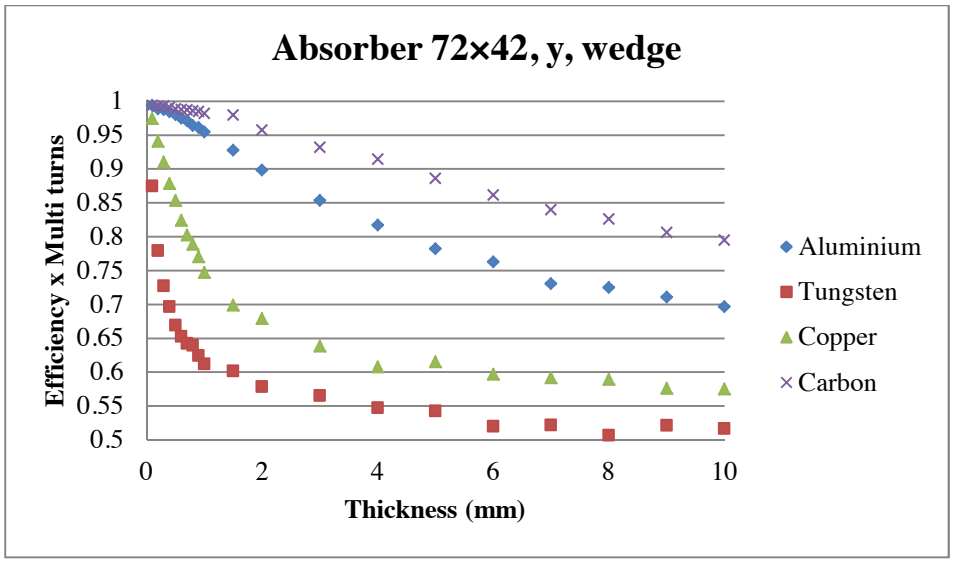

Figure 16: *A possible alternative to having thresholds for efficiency and multi turns is to multiply the two together. The horizontal phase space has slightly better results and is therefore not the limiting factor.*

4.2 1.4 GeV Simulations

Material	Efficiency	RMS scattering angle (mrad)
Graphite flat x 0.1mm	1	0.115
Graphite flat x 0.2mm	0.9999*	0.168
Aluminium flat x 0.1mm	1	0.176
Tungsten wedge x 0.1mm	1	0.114
Graphite flat y 0.1mm	1	0.115
Graphite flat y 0.2mm	1	0.168
Aluminium flat y 0.1mm	1	0.176
Tungsten wedge y 0.1mm	0.9999	0.114

Table 2: *Flat scraper and tungsten wedge, these were not plotted because there are not enough data points to justify graphs. 0.9999 as opposed to 1 is significant as it indicates the scraper design is on the edge of maximum efficiency. Multi turns are not included as these are all 1.*

Table 2 presents the values of the RMS scattering angles at the thicknesses used. Thicknesses were chosen for similar performance at 160 MeV, the scattering angles all being broadly similar at 1.4 GeV indicates similar performance at extraction energy too.

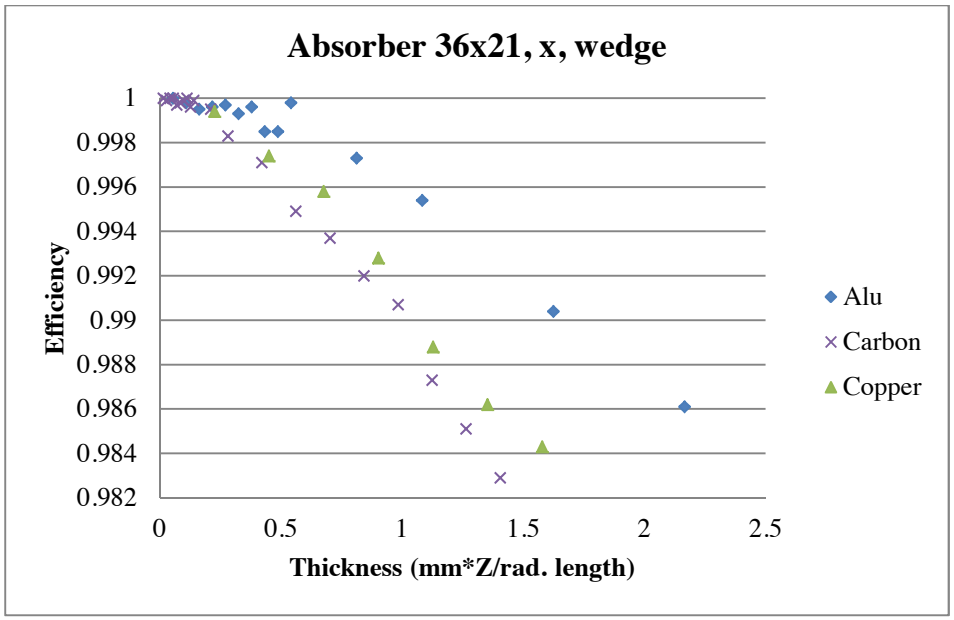

***Figure 17**: The efficiency for particles lost in horizontal phase space. The x axis is corrected for radiation length and nuclear charge, as is figure 18.*

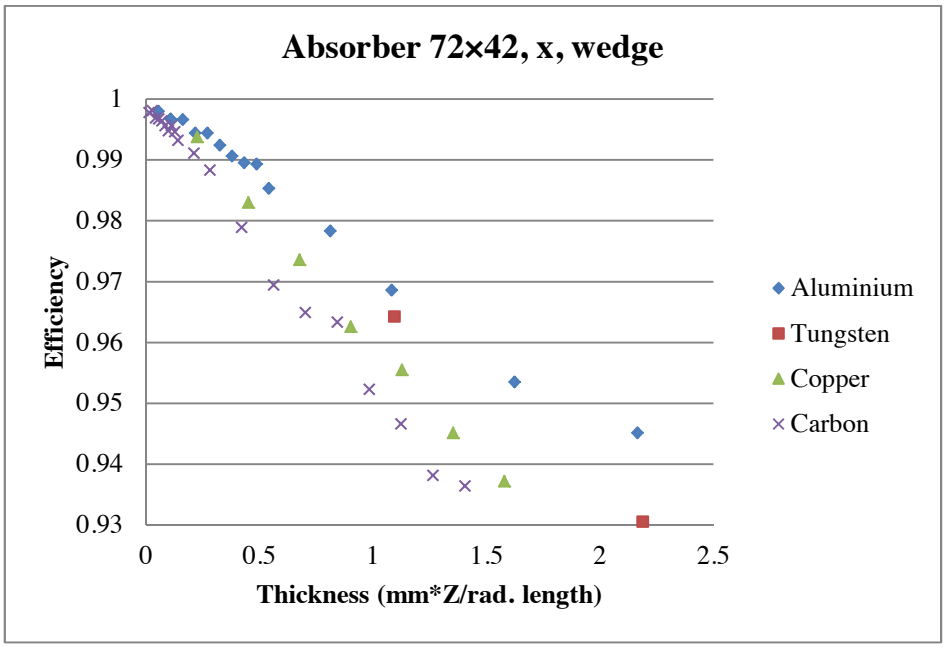

***Figure 18**: Efficiency at 160 MeV over the same range of thicknesses for comparison.*

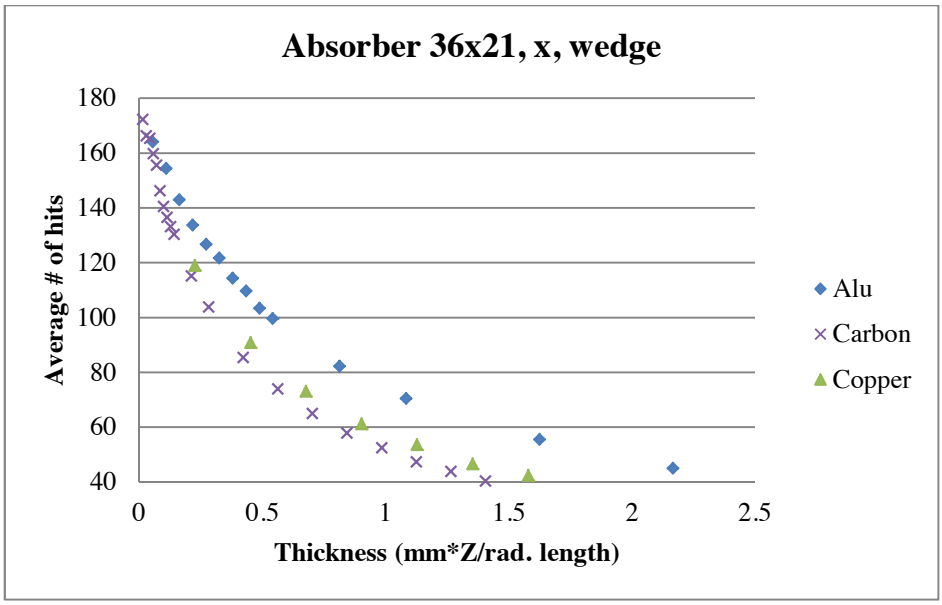

***Figure 19**: Average number of hits on the scraper for horizontal phase space.*

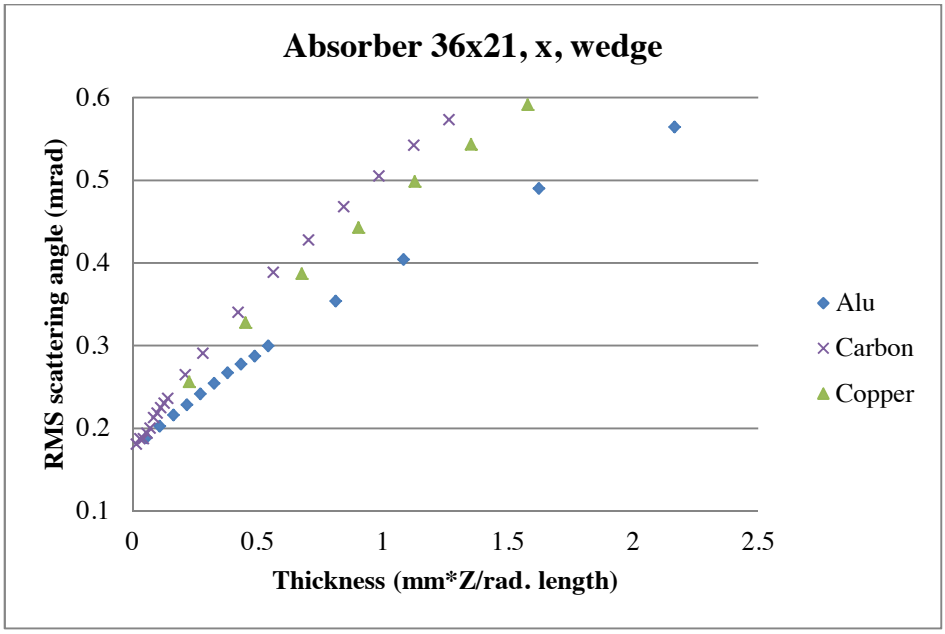

***Figure 20**: RMS scattering angle at 1.4 GeV.*

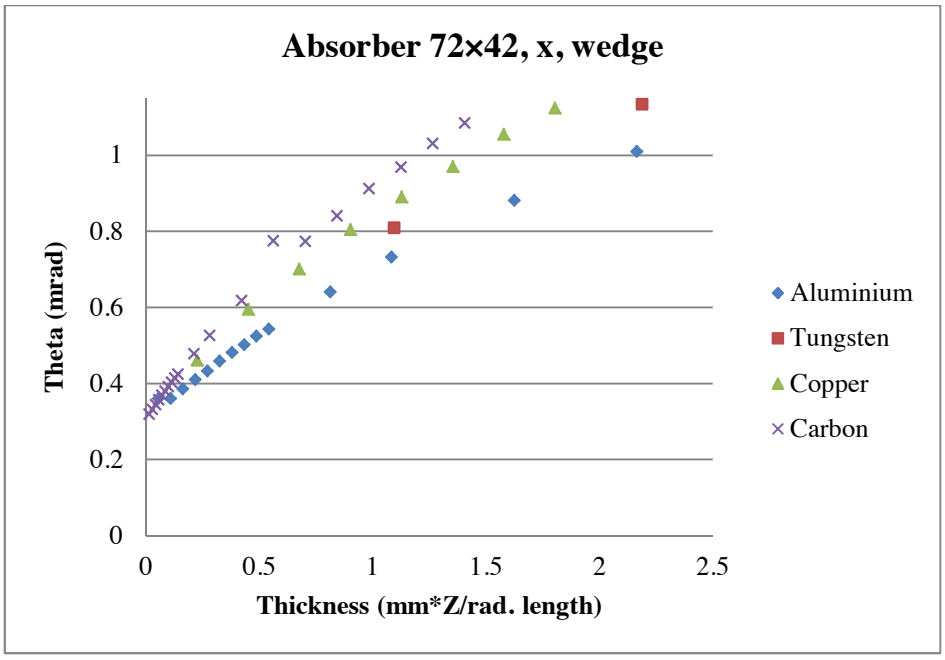

***Figure 21**: Scattering angle at 160 MeV.*

At 1.4 GeV, the RMS scattering angles become much smaller (compare figure 20 to figure 21) which in some respects makes the scraper behave equivalent to a thinner one than it did at 160 MeV. For example, at 160 MeV in figure 17, graphite has an efficiency of just over 98% for a 1.5mm scraper, at 1.4 GeV in figure 18 it would have this efficiency at around 0.4mm and the whole 0-2.5mm range of figure 17 resembles the roughly 0-0.5mm portion of figure 18.

Performance at 1.4 GeV is significantly better than 160 MeV, so that the scraper choice can be made on the basis of efficiency and multi turns at the injection energy. The larger number of hits on the scraper places limits on the design due to the amount of heat the scraper may be subjected to.

4.3 Tune Variation

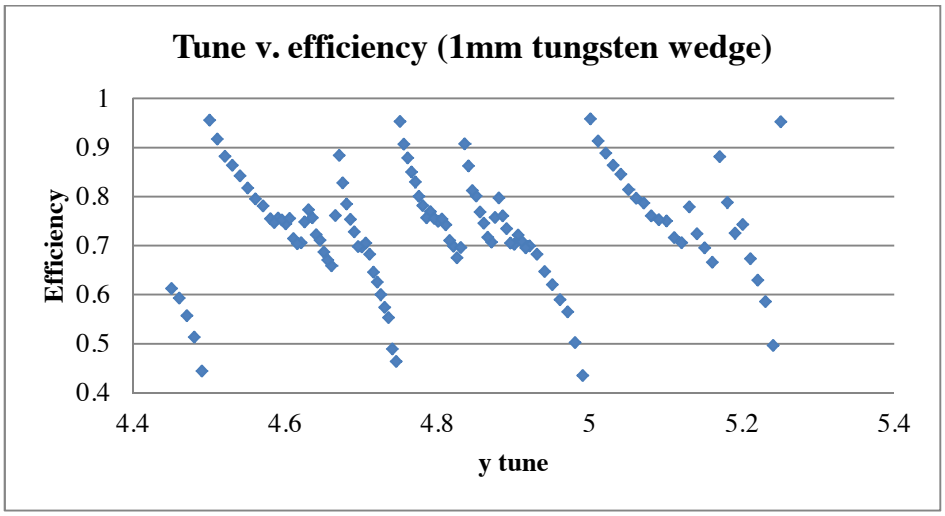

***Figure 22**: The efficiency of the tungsten wedge scraper over the full range investigated. The 5.0 – 5.3 section looks the same as 4.5 – 4.8 and 4.45 – 4.5 looks likely to be part of the same shape just below 5.0.*

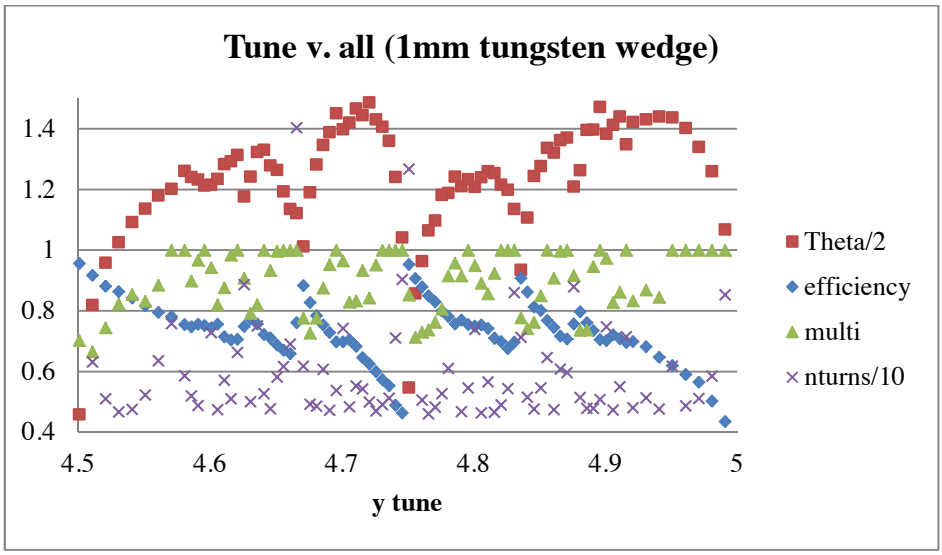

***Figure 23**: The tungsten wedge in detail over a range of 0.5 in* y *tune. Scattering angle, efficiency, multi turns and average number of hits (*nturns*) have been plotted on the same graph to show how they correlate. The average number of hits has been divided by 10 and the scattering angle by two in order to put them in a similar range to the other parameters.*

The tungsten wedge (figure 22) shows a repeating pattern over a range in tunes of 0.5. The range 4.5 to 5 was investigated in more detail with smaller increments of 0.005 (figure 23). This is not the most likely range of the machine tune but the pattern looks probably identical over any range of 0.5. From looking at the scattering angle, it picks out resonances at (subtracting the starting point of 4.5 and in approximate order of significance) 1/4, 1/6, 1/3, 1/8, 3/8, 1/10, 1/5, 0.216, 3/10, 0.421, 3/40, and 1/7. Most of these are obvious integer or fractional resonances, some less so but might be more sensible fractional resonances not obvious from the resolution of the graph, or not on the pattern that repeats every 0.5. Only the major resonances were clearly repeating every 0.5, the more subtle ones were only noticed when it was looked at in detail over a smaller range.

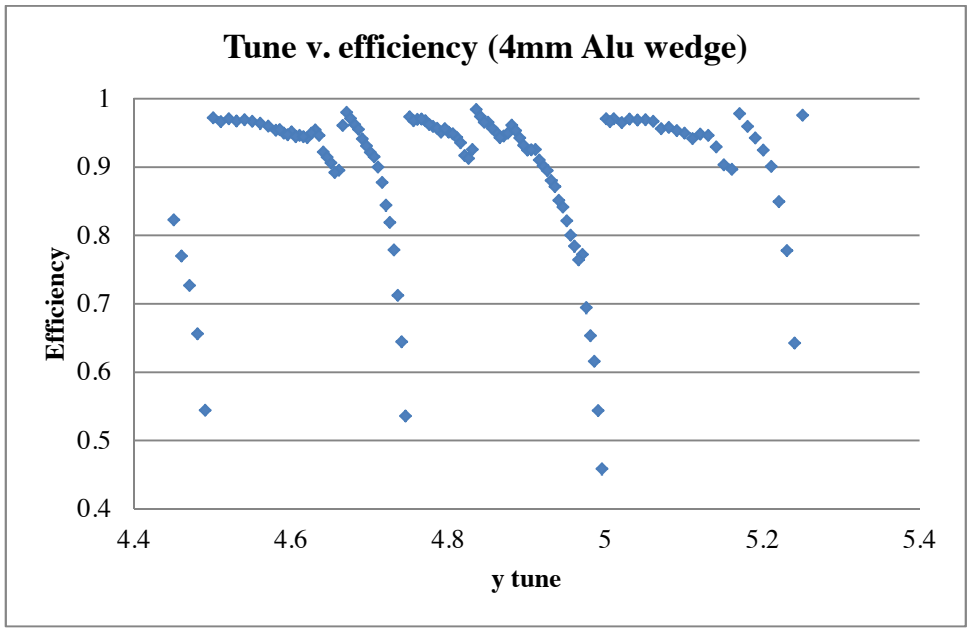

***Figure 24**: Tune for the aluminium wedge. The pattern is very similar to the tungsten wedge (figure 22) but with efficiencies concentrated higher.*

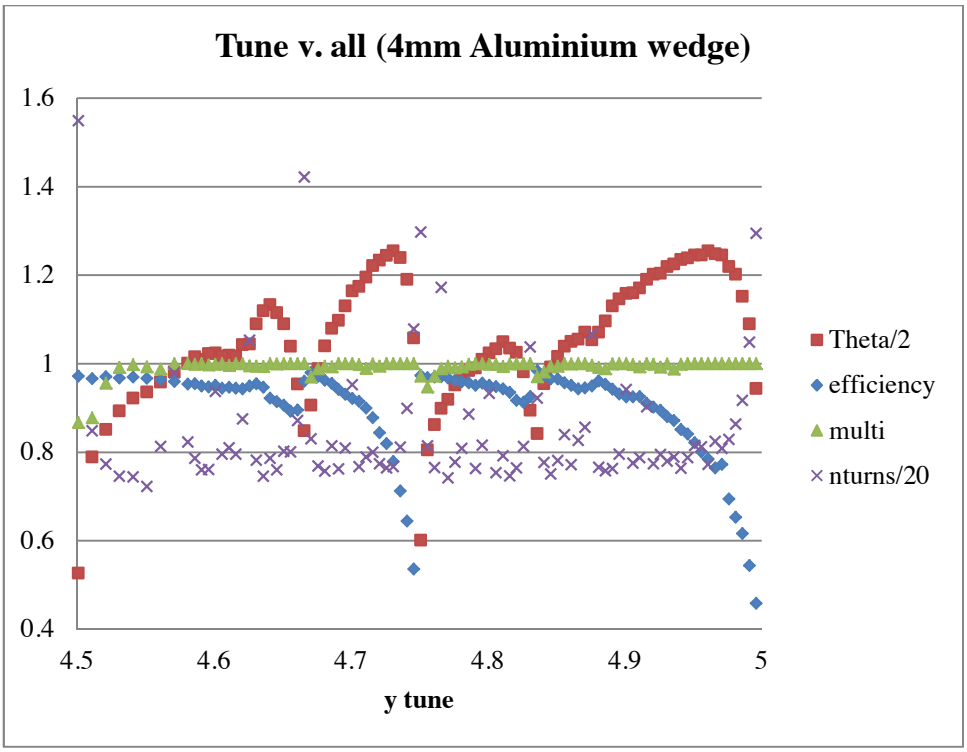

***Figure 25**: As figure 23, for the aluminium wedge.*

Not plotted: Tungsten, flat, 0.1mm. All tunes have efficiency 0.83, average number of hits 1.02, multi turns 0.004 – 0.023.

The aluminium wedge pattern (figures 24 – 25) looks very similar to the tungsten wedge but with not quite as many resonances. This is probably because the efficiencies are all quite high so are harder to identify. Resonances picked out from the scattering angle graphs are 1/4, 1/6, 1/3, 1/9, 3/8 and 7/25. The resonances at 1/9 and 7/25 are less obvious on the tungsten scraper, which also has some features not on the plot of the aluminium scraper.

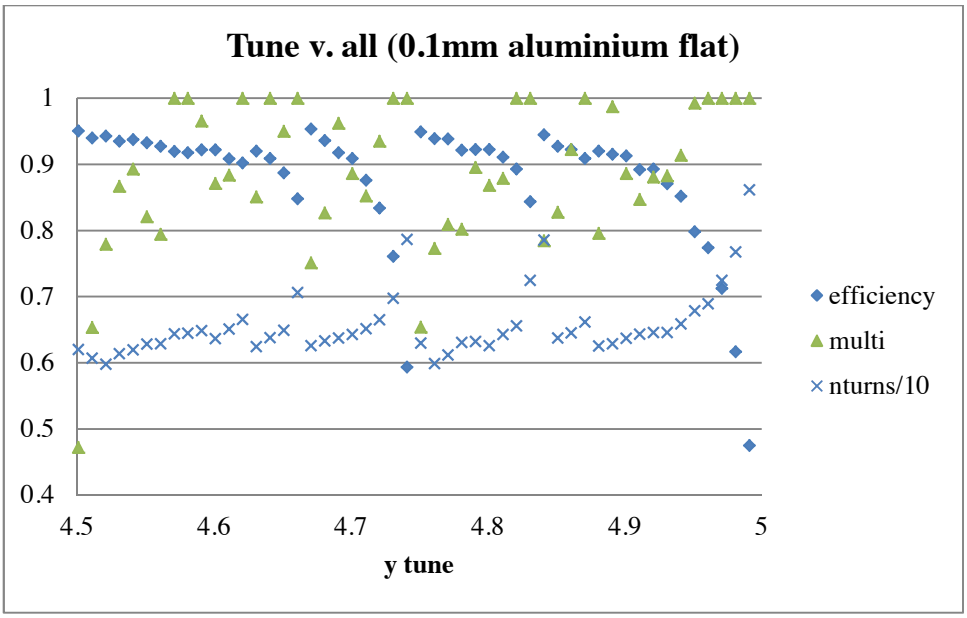

***Figure 26**: As figure 23, but for the flat aluminium scraper. Scattering angle has been removed as this is constant.*

The flat aluminium scraper (figure 26) has similar variations to the wedge scrapers. This indicates that whatever is causing the variations is not the thickness of scraper traversed, which otherwise would have been a good explanation for the behaviour of the wedge. The only difference between wedge and flat seems to be whether multi turns or number of hits has a stronger correlation with the efficiency. For the tungsten wedge (figures 22 - 23) there is a strong correlation between the scattering angle and efficiency, they mainly mirror each other (one increases when the other decreases) except some very large dips in scattering angle correlate to a dip rather than a peak in efficiency. For the flat aluminium (figure 26) the scattering angle is fixed. For the tungsten wedge (figures 22 - 23) scraper the average number of hits looks almost random and multi turns do not look much more closely correlated, there are a couple of groups of around 100% multi turns which tend to be where the scattering angle and efficiency are decreasing. The flat aluminium (figure 26) on the other hand has the number of hits mirroring the efficiency. Most dips in efficiency look loosely correlated with the high

fraction of multi turns but there are also very high multi turns in other places. It is not clear why there is so little correlation between average number of hits and multi turns, or why average number of hits had such a strong correlation with efficiency in the flat case but not the wedge.

For both flat and wedge scrapers the tune must be accurately known as for a given design the tune can make the difference between an efficiency of 95% and 85%, even lower on or very near a 1/4 integer (including 1/2 integer and integer) resonance. When the tune is known, it is possible that a thinner (to get adequate efficiency) or thicker (for better robustness if there is a good margin for the efficiency) scraper may be better than the one proposed for the currently assumed tune.

The most significant result from this is the way the efficiency changes with tune does not follow a smooth, predictable pattern but has some very sudden changes. A detailed simulation will have to be run for the actual tune when it is finalised, results cannot be extrapolated from similar tunes.

The similarity between both wedges suggests that the difference in performance from the flat aluminium scraper indicates that geometry alone dictates the behaviour, a scraper of similar performance but another material shows the same pattern. The effects seen probably occur because tunes near resonances result in higher betatron oscillations. This means any particles which do not go straight into the absorber are more likely to be lost in the machine as they are more likely to oscillate outside the acceptance.

4.4 Heating

Material	Thick ness	Hits	Effic iency (160 MeV)	Multi turns (160 MeV)	Temp 2×10^{13} pcls (K) 1.4GeV	Temp 2×10^{13} pcls (K) 160MeV	Melts (K)	n	Ratio to melting point	total time (ms)	Mel- ting time (ms)
Beryllium	0.4	155	0.7951	0.9916	2325	522	1560	152	1.49	0.809	0.621
Graphite	0.2	170	0.806	0.9931	6727	944	3948	170	1.70	0.904	0.555
Alu	0.1	155	0.7929	0.9923	4333	736	933.5	155	4.64	0.824	0.19
Copper	0.02	123	0.7543	0.9817	6901	1188	1358	123	5.08	0.654	0.134
Tungsten	0.005	121	0.7544	0.9783	15175	2275	3695	121	4.11	0.644	0.16
Lithium	0.1	157	0.7831	0.9888	1231	409	453.6	142	2.71	0.755	0.365
Boron	0.06	156	0.8075	0.9832	4043	708	2349	157	1.72	0.835	0.523
Diamond	0.2	169	0.8169	0.9944	8965	1183	3820	169	2.35	0.899	0.396

Table 3: *How much each material is heated by a beam loss. No conduction, radiation, variable heat capacities or increased thicknesses to reduce hits are taken into account.*

The first column of data in table 3 gives the desired thickness of the scraper in mm giving around 80% efficiency. A lower efficiency is tolerated for copper and tungsten due to the very low thicknesses involved, and also because for copper and tungsten a wedge may work better and these thicknesses are approximating a wedge of slightly better efficiency, for which it would be much more difficult to calculate the heating. All scrapers here are flat for ease of calculating the heating, although wedges have not been ruled out. Hits is the average number of times a particle will hit that scraper design, temperatures for 160 MeV assume 7 hits as all materials showed an average number of hits between 5 and 7 at 160 MeV. The upper bound was taken because the main purpose of the 160 MeV temperatures are to show they are lower than at 1.4 GeV. The higher energy loss per hit at 160 MeV is less important than the larger number of hits at 1.4 GeV.

The sixth and seventh columns are the temperatures assuming 2×10^{13} particles for beam losses at 160 MeV and 1.4 GeV. The temperature assumes no conduction as this has been shown to make no noticeable difference to the maximum temperature.

The tenth column is the ratio between the maximum temperature and the melting point of the material. The best of these is Beryllium, but even then 50% over the melting point. Beryllium also has the smallest absolute difference between maximum temperature and melting point but still probably too much for a cooling system to make a difference. Lithium has the lowest final temperature but slightly higher absolute difference from melting point, much higher ratio to the melting point, shorter time to reach the melting point but is not a suitable material for a scraper.

With the geometry here a mechanism to remove the beam before it melts the scraper would be needed. From the time taken to lose the particle and the temperature then, the time after the particles first hit the scraper when the melting point is reached can be calculated. Again, the best of these is Beryllium at 0.621ms, graphite and boron are not far behind at around 0.5ms. However, boron was only included to show low Z behaviour and is not a practical material to create a scraper out of, but boron carbide might be worth investigating.

4.5 Conduction

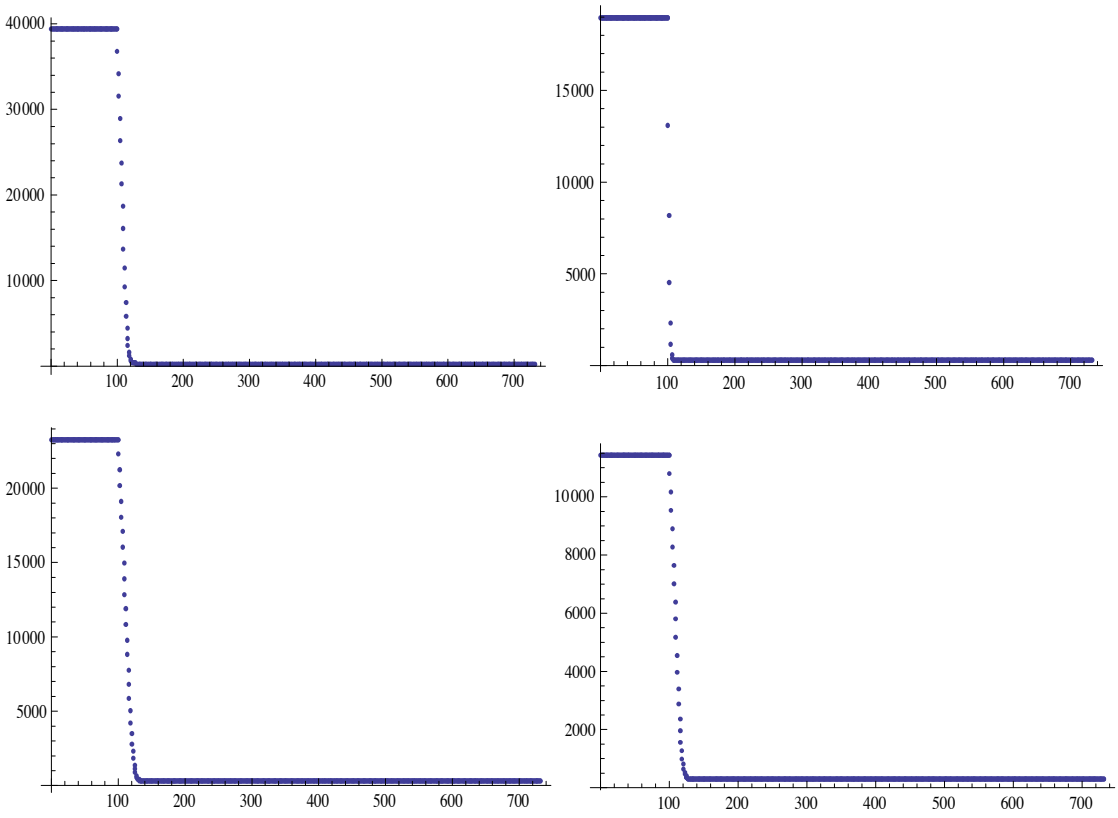

Figure 27: *These graphs are what happens after 3640 time iterations of input beam, the expected time the beam would be on the scraper. The y axis is temperature in Kelvin, the x axis is element number (see Appendix 3). Top row (left to right): tungsten and graphite. Bottom row: copper and aluminium.*

Simulations with conduction indicated some cooling at the edge of the beam but made no difference to the centre, meaning that the maximum temperature was not affected. Therefore conduction will not be considered as a factor in calculating whether the scraper will melt.

4.6 Radiation

Material	Emissivity	Radiated power (J)	Input power (J)	Radiated/input
Aluminium	0.02	0.017	3.0×10^{4}	5.9×10^{-7}
Tungsten	0.02	4.33	4850	8.9×10^{-4}
Copper	0.02	0.079	2.16×10^{4}	3.7×10^{-6}
Graphite	0.75	53.2	7.14×10^{4}	7.4×10^{-4}
Diamond	0.02	2.4	1.63×10^{5}	1.5×10^{-5}
Boron	0.9	31.9	6.95×10^{4}	4.6×10^{-4}
Lithium	0.02	9.8×10^{-4}	1.4×10^{5}	7.0×10^{-9}
Beryllium	0.02	0.14	8.54×10^{4}	1.6×10^{-6}

Table 4: *the power radiated at melting temperature (found using the Stefan-Boltzmann law) compared with the input power from the incident beam (from the Bethe equation only).* [42][43][44]

The highest fraction of any radiated power as a proportion of the input power is about 0.1% making this negligible as a cooling effect. Due to the approximations involved this is actually an overestimate, making the real radiated power of even less significance. Heat loss by radiation will therefore be disregarded.

4.7 Variable Heat Capacities

Material	Temp fixed C (K)	Temp variable C (K)	Melting point	Melts?
Graphite	6727	2795	3948	No
Diamond	8965	3186	3820	No
Copper	6901	5452	1358	Yes but later

Table 5: *New temperatures calculated from heat capacities which change significantly with temperature. This is only significant above room temperature for carbon and copper.*

The temperature dependent heat capacity (table 5) gave a 21% reduction in maximum temperature for the copper scraper, but this was not enough to prevent melting. It does however delay the point at which it melts, since the beam would have to be stopped in under 23 hits as opposed to 19 as indicated by the constant value heat capacity. If one turn of the PSB is 10^{-6}s and 18.8% of the turns result in a hit, 23 hits is about 120μs.

As the melting point is the maximum value covered by the data in [37], whether or not the extrapolation beyond there is accurate does not matter.

The graphite and diamond scrapers however are safely below their melting/sublimation points making these appear viable. More accurate data on how heat capacity changes at high temperatures is needed to confirm this as [38] only gives figures up to 1500K and the formulae have been assumed to hold up to 2000K for graphite and 2428K for diamond.

4.8 Reducing the Number of Turns

Material	Hits	New hits	Old thickness (mm)	New thick. (mm)	Efficiency	New Eff.	Eff. × multi
Aluminium	155	77	0.1	0.2	0.6568	0.6568	0.61483048
Copper	123	20	0.02	0.14	0.5102	0.5102	0.28719158
Tungsten	121	45	0.005	0.014	0.5671	0.5671	0.4616194
Beryllium	155	96	0.4	0.66	0.6930	0.6930	0.6631317
Lithium	157	48	1.8	6.0	0.5723	0.5723	0.47460839
Boron	156	102	0.25	0.38	0.7115	0.7115	0.6878782

Table 6: *Performance for scrapers with thickness increased to that which would not result in heating from a beam loss melting the scraper.*

Most of the scrapers tried here would appear to melt according to tables 3 and 5, but if poorer efficiency can be tolerated then it is possible to modify the beryllium or even aluminium scraper to something which would not melt. Beryllium only shows a 3.6% improvement on aluminium, which may not enough to justify it given the significant safety concerns. Lithium and Boron were only included to indicate low Z behaviour.

4.9 Nuclear Scattering

Material	Nuclear events: 1.4 GeV	160 MeV	Energy loss: 160 MeV (J)	Energy loss: 1.4 GeV (J)	B-B energy loss (J) (1.4 GeV)
Aluminium	2.42×10^{11}	3.07×10^{11}	15.72	54.21	11.3
Graphite	5.18×10^{11}	6.36×10^{11}	32.58	116.3	22.6
Diamond	8.26×10^{11}	1.01×10^{12}	51.88	185.2	35.8
Copper	1.21×10^{11}	1.60×10^{11}	8.223	27.07	5.26
Tungsten	4.56×10^{10}	6.66×10^{10}	3.412	10.23	2.22
Beryllium	9.54×10^{11}	1.30×10^{12}	66.54	214.1	31.56
Lithium	1.35×10^{11}	1.88×10^{12}	96.33	303.7	41.3
Boron	7.47×10^{11}	9.83×10^{11}	50.38	167.6	27.1

Table 7: *Number of nuclear scattering events and the energy loss they result in, assuming all kinetic energy of the particle is deposited in the scraper.*

More detailed simulations need to be done on the effects of nuclear scattering, if the energy from these scatters (about a factor of five greater than that due to ionisation for most materials, and around 7 for very low atomic numbers) all counts towards heating then they will be a serious and possibly insurmountable problem. If the debris from these events leaves the scraper depositing almost no energy their effect will be almost negligible. To establish which of these scenarios or what combination of them is the case will require an extensive custom Monte Carlo generator beyond the scope of this project. It is possible that if nuclear losses are significant, in which case it may have to be checked if a thicker diamond scraper could still have useful performance.

4.10 Accuracy and Errors

Nothing in this thesis has been experimentally verified so there could still be important effects and practical issues which haven't been thought of yet. All simulations have been custom written and might still contain mistakes. This study mainly serves the purpose to indicate what needs looking into in more detail such as by more rigorous simulation and testing with a live beam. There is no current similar protection system in the PSB to compare against.

There are several known sources of error:

- The beam size is very difficult to measure accurately and it is even harder to predict the exact size in a machine which hasn't been built yet.
- The tracking around the machine is a very simplified model.
- Only two initial particle trajectories have been considered.
- The Bethe-Bloch equation is an approximation for a narrow range of energies
- The RMS scattering angle has been assumed to have a Gaussian distribution; this is a very approximate model of its distribution.
- The simulations have been run for enough turn to find how almost all particles are lost, this involves running it for longer than the machine would have them at that energy for which might bias it in favour of slower loss methods.
- The manufacturing errors are at least 0.01mm [41], positioning is probably about 0.1mm if it can be adjustable.
- The exact motion of the beam during a loss has not been carefully modelled.
- The beam has been approximated to simpler distributions for heating simulations.
- Conduction may change with temperature
- Material imperfections will probably matter

These generally result in pessimistic estimates or are expected to be small.

5. Conclusions

5.1 Performance and Design

Graphite	Flat 0.2mm	Wedge 10+mm
Aluminium	Flat 0.1mm	Wedge 4mm
Tungsten	Flat N/A	Wedge 0.1mm
Copper	Flat N/A	Wedge 0.7mm.
Beryillium	Flat 0.4mm	
Diamond	Flat 0.2mm	
Lithium	Flat 1.8mm	
Boron	Flat 0.25	

Table 8: *Maximum acceptable scraper thicknesses using the graphs of efficiency × multi turns (figure 16) and an efficiency × multi turns threshold of 0.8.*

All thicknesses quoted are the maximum acceptable according to this study. More detailed simulations could change these figures. Wedge thicknesses were not established for the lower four materials as these materials were only investigated after the heating concerns arose; the lack of conduction on relevant timescales makes the thin point of a wedge very vulnerable as well as much harder to model, so only flat scrapers were used from then onwards.

From this alone, the 4mm aluminium wedge or 0.5mm copper would look likely to be best. A 0.1mm flat sheet of aluminium would be a lot more robust at the point where the particles hit.

If worse performance could be tolerated, some materials could satisfy this at thicknesses which would not appear to melt them.

5.2 Overall Conclusion

In the event of a beam loss depositing the maximum possible energy on the scraper, taking into account only Bethe-Bloch losses, one can theoretically propose a high performance scraper made from graphite or diamond and a reasonable one made from aluminium. Practical considerations rule out graphite, since above 70°C it outgasses and degrades the vacuum. This leaves either diamond or finding a way to ensure that the worst case scenario discussed here does not happen. [45]

A tungsten scraper is unrealistically thin and should probably be disregarded even if a fast kicker renders its performance acceptable. Brief research on the internet did not find a source of tungsten at the required thickness but sheet or foils for all other scrapers investigated here appear to be obtainable.

Diamond has the best material properties for the scraper as established in this study, although the practical and economic concerns of constructing a suitable scraper have not been investigated.

The option least likely to hit practical or economic barriers is aluminium, but this requires reduced performance or something to ensure the entire beam is never lost on the scraper.

All of this depends on a more in-depth look at the effects of nuclear scattering, which could result in the heating being anywhere up to eight times higher, but it could also be low enough to not make much difference.

6. Appendices

Appendix 1: *Mathematica* Tracking Code

```
(*material={z, rho, x0, Io, A}*)
Tungsten = {74, 19.3, 3.5, 741.5351*10^-6, 183.84};
Aluminium = {13, 2.699, 88.96, 161.8284*10^-6, 26.9815386};
Copper = {29, 8.96, 14.35, 311.4414*10^-6,  63.546};
Carbon = {6, 2.21, 193.2, 79*10^-6, 12.0107};
Beryllium = {4, 1.848, 352.8, 55*10^-6, 9.012182}; (*was 58*)
Lithium = {3, 0.534, 1550.19, 46.3*10^-6, 6.9412};
Boron = {5, 2.46, 216.26, 69.7*10^-6, 10.811};
CDiamond = {6, 3.52, 121.3, 79*10^-6, 12.0107};
(*Energy={beta, gamma, mom, ke}*)
onesixty = {0.52, 1.17, 570.75, 160};
onepfour = {0.9159915293879254, 2.4925373134328357, 2141.5881957089696, 1400};
twogev = {0.94767, 3.1322, 2784.2414 , 2000};
(*Set up variables*)
Tracking12[{A1_, B1_, A2_, B2_, mu1_, mu2_, xtune_}, {A1y_, B1y_, A2y_, B2y_, mu1y_,
mu2y_, ytune_}, {accepx_, accepy_, disp_, xin_, yin_, delpp_, nturn_}, {a_, b_, absx_, absy_},
{dels_, dela_, delb_}, {z_, rho_, X0_, Io_, A_}, {beta_, gamma_, mom_, ke_}] :=
 (*Create module to internally do calculations*)
 Module[{r = {xin, 0, yin, 0, delpp}, r1s = {}, hits1 = {}, hits2 = {}, r2s = {}, outsidex = {},
outsidey = {}, hitabs = {}, lastvector = {}, theta = {}},
  (*Initialise variables*)
  psi21 = xtune*Pi*2 - (mu2 - mu1);
  psi21y = ytune*Pi*2 - (mu2y - mu1y);
  (*de/dx, needs to be multiplied by density*)
  dEbyDx = (0.307*z/(A*beta^2))*(Log[(2*0.511*beta^2*gamma^2)/Io] - 0.5*Log[1 +
2*gamma/1836 + 1/1836^2] - beta^2);
  (*RMS scattering angle*)
   thetarms = (13600/(beta*mom))*Sqrt[dels/X0]*(1 + 0.038*Log[dels/X0]);
  theta = thetarms;
  (*Matrices: 12 is point 1 to 2, 21 is back to 1, in x and y*)
  M12 = {{Sqrt[B2/B1]*(Cos[mu2 - mu1] + A1*Sin[mu2 - mu1]), Sqrt[B1*B2]*Sin[mu2 -
mu1]}, {-((1 + A1*A2)/Sqrt[B1*B2])*Sin[mu2 - mu1] + ((A1 - A2)/Sqrt[B1*B2])*Cos[mu2 -
mu1], Sqrt[B1/B2]*(Cos[mu2 - mu1] - A2*Sin[mu2 - mu1])}};
  M21 = {{Sqrt[B1/B2] (Cos[psi21] + A2*Sin[psi21]), Sqrt[B2*B1]*Sin[psi21]}, {-((1 +
A2*A1)/Sqrt[B2*B1])*Sin[psi21] + ((A2 - A1)/Sqrt[B2*B1])*Cos[psi21],
Sqrt[B2/B1]*(Cos[psi21] - A1*Sin[psi21])}};
  M12y = {{Sqrt[B2y/B1y]*(Cos[mu2y - mu1y] + A1y*Sin[mu2y - mu1y]), Sqrt[B1y*B2y]*
     Sin[mu2y - mu1y]}, {-((1 + A1y*A2y)/Sqrt[B1y*B2y])*Sin[mu2y - mu1y] + ((A1y -
A2y)/Sqrt[B1y*B2y])*Cos[mu2y - mu1y], Sqrt[B1y/B2y]*(Cos[mu2y - mu1y] -
A2y*Sin[mu2y - mu1y])}};
  M21y = {{Sqrt[B1y/B2y] (Cos[psi21y] + A2y*Sin[psi21y]), Sqrt[B2y*B1y]*Sin[psi21y]}, {-
((1 + A2y*A1y)/Sqrt[B2y*B1y])*Sin[psi21y] + ((A2y - A1y)/Sqrt[B2y*B1y])*Cos[psi21y],
Sqrt[B2y/B1y]*(Cos[psi21y] - A1y*Sin[psi21y])}};
  (*Dispersion*)
```

```
  {Dx, Dxpri} = {disp, 0} - M12.{disp, 0};
  {Dx2, Dx2pri} = {disp, 0} - M21.{disp, 0};
  (*Put the x and y matrices together*)
  M512 = {{M12[[1, 1]], M12[[1, 2]], 0, 0, Dx}, {M12[[2, 1]], M12[[2, 2]], 0, 0, Dxpri}, {0, 0,
M12y[[1, 1]], M12y[[1, 2]], 0}, {0, 0, M12y[[2, 1]], M12y[[2, 2]], 0}, {0, 0, 0, 0, 1}};
  M521 = {{M21[[1, 1]], M21[[1, 2]], 0, 0, Dx2}, {M21[[2, 1]],  M21[[2, 2]], 0, 0, Dx2pri}, {0,
0, M21y[[1, 1]], M21y[[1, 2]], 0}, {0, 0, M21y[[2, 1]], M21y[[2, 2]], 0}, {0, 0, 0, 0, 1}};
  (*Loop starts here*)
  (*First if statement checks if particle hits collimator*)
  Do[If[a + dela > Abs[r[[1]]] > a || b + delb > Abs[r[[3]]] > b,
   (*Updates vector with particle motion properties*)
   (*0.37=1/beta^2 * 0.1 (cm^-1 -> mm^-1), 1098=KE+M *)
   (*why divide by beta^2??*)

   r = r + {0, RandomReal[NormalDistribution[0, thetarms]], 0,
RandomReal[NormalDistribution[0, thetarms]],  dEbyDx*(0.1/(beta^2))*dels*rho/(938 + ke)};
   (*Logs what happened so it can be viewed outside the module*)
            AppendTo[hits1, {indturn}]];
  (*Moves particle on to absorber block*)
       r = M512.r; AppendTo[r2s, r];
  (*Checks if it hits, if so, logs and stops*)
       If[Abs[r[[1]]] > absx || Abs[r[[3]]] > absy, AppendTo[hitabs, indturn];
AppendTo[lastvector, r]; Break[],
   (*If not, same for getting lost in machine*)
   If[((1 + A2y*A2y)/B2y)*(r[[3]])^2 + 2*A2y*(r[[3]])*(r[[4]]) + B2y*(r[[4]])^2 > accepy,
AppendTo[outsidey, indturn]; AppendTo[lastvector, r]; Break[]];
   If[Sqrt[((1 + A2*A2)/B2)*(r[[1]] - disp*delpp)^2 + 2*A2*(r[[1]] - disp*delpp)*(r[[2]]) +
B2*(r[[2]])^2] > Sqrt[accepx] - Abs[r[[5]]]*disp/Sqrt[B2],  AppendTo[outsidex, indturn];
AppendTo[lastvector, r]; Break[]];
   (*If not hit absorber or lost, particle continues back to start. Logs vector and information for
graph plotting*)
   r = M521.r; AppendTo[r1s, r]],
      {indturn, 1, nturn}];
  hits2 = Length[hits1];(*Dimensions[hits1];*)
  lastel = hits1[[hits2]];
  frac = hits2/lastel;
  (*Outputs information*)
  {r1s , r2s, hits1, outsidex, outsidey, hitabs, lastvector, hits2, frac, theta} ]
data = Table[Tracking12[{1/6, 6., -1/6, 6., 0., 2/6, 4.281}, {1/5, 5., -1/5, 5., 0, 2/5, 4.451}, {365,
120, 1.4, 1, 18, 0, 1000000}, {33, 18, 36, 21}, {0.015, 100, 100}, Tungsten, onesixty][[{4, 5, 6 ,
8, 9, -1}]], {10000}];
{xacc, yacc, abs, hits, fract, tharmss} = Transpose[data];
{xloss, yloss, absloss} = {Join @@ xacc, Join @@ yacc, Join @@ abs};
Dimensions[absloss]/(Dimensions[yloss] + Dimensions[xloss] + Dimensions[absloss])
Dimensions[yloss];
Dimensions[xloss];
Dimensions[absloss];
theta = Mean[tharmss];
f = Total[#] > 10 &;
outp = Select[abs, f];
absturn = Join @@ outp;
```

```
Dimensions[absturn]/Dimensions[absloss]
theta
N[Mean[fract]]
N[Mean[hits]]
```

Appendix 2: *Mathematica* Code for Conduction

```
(*Copper*)
(*cv=0.384928;
k=3.93296;
dels=0.002;
Pa=43603;
rho=8.96;*)
(*Aluminium*)
(*cv=0.89956;
k=2.21752;
dels=0.01;
Pa=74438;
rho=2.699;*)
(*Carbon*)
(*cv=0.69036;
k=0.238488;
dels=0.02;
Pa=156755;
rho=2.21;*)
(*Diamond*)
cv = 0.5091928;
k = 23.2;
(*k=23.2;*)
dels = 0.02;
Pa = 191615;
rho = 3.52;
(*Beryllium*)
(*cv=1.824224;
k=1.58992;
dels=4;
Pa=207960.0;
rho=1.848;*)
(*Tungsten*)
(*cv=0.133888;
k=2.00832;
dels=0.05;
Pa=206946.3;
(*138793.0;*)
rho=19.3;*)
t = ConstantArray[293.0, 732];
Temp = ConstantArray[293.0, 732];
(*Find out how many elements to edge of effective beam*)
(*Check power calculation*)
(*number of elements the beam hits*)
```

```
m = 100;
(*size of element in radius*)
delr = 0.01368;
(*time increment*)
delti = 10^-6;
Do[t[[1]] =Temp[[1]] + (Pa*delti)/(dels*cv*rho) -k*delti*2*n*(Temp[[2]] -
Temp[[1]])/(delr^2*rho*cv);
 For [n = 2, n < 731, n++,
  If[ n <= m,
   t[[n]] = Temp[[n]] + (Pa*delti)/(dels*cv*rho) + k*delti*2*((n - 1) (Temp[[n - 1]] - Temp[[n]])
- n (Temp[[n]] - Temp[[n + 1]]))/(delr^2*rho*cv*(2*n - 1)),
t[[n]] = Temp[[n]] + k*delti*2*((n - 1) (Temp[[n - 1]] - Temp[[n]]) - n (Temp[[n]] - Temp[[n +
1]]))/(delr^2*rho*cv*(2*n - 1))]];
 Temp = t, {3640}];
(*Cooling when the beam is off*)
Do[t[[1]] =Temp[[1]] - k*delti*2*n*(Temp[[2]] - Temp[[1]])/(delr^2*rho*cv);
 For [n = 2, n < 731, n++,
t[[n]] = Temp[[n]] + k*delti*2*((n - 1) (Temp[[n - 1]] - Temp[[n]]) - n (Temp[[n]] - Temp[[n +
1]]))/(delr^2*rho*cv*(2*n - 1))];
 Temp = t, {30000}];
```

Appendix 3: *Mathematica* Code for Variable Heat Capacities

Note: the code for heating with no conduction and fixed heat capacity was very similar but with the fixed value instead of the heat capacity calculation.

```
z=6;
A=12.0107;
Io=79;
rho=2.21;
dels=0.2;
turns=310;
beta=0.94767;
gamma=3.1322;
T=293;
For [n=1 , n<257,n++,
 If [T<2000,c=11/120+0.0004T-10^-7*T^2,c=59/120];
 delt=2*(0.307*z/(A*beta^2))*(Log[(2*0.511*beta^2*gamma^2)/(Io*10^-6)]-
0.5*Log[1+2*gamma/1836+1/1836^2]-
beta^2)*0.1*dels*rho*1.60217646/(rho*0.2304*dels*0.1*c*4.184);
 T=T+delt]
T
```

Appendix 4: *Mathematica* Code for Nuclear Scattering

```
(*sigmas here: http://pdg.lbl.gov/2010/hadronic-xsections/pp_total.dat *)
(*Graphite*)
(*rho=2.21;
dels=0.02;
Am=12.0107;
z=6;*)
(*Diamond*)
(*rho=3.52;
dels=0.02;
Am=12.0107;
z=6;*)
(*Copper*)
(*rho=8.96;
dels=0.002;
Am=63.546;
z=29;*)
(*Aluminium*)
(*rho=2.699;
dels=0.01;
Am=26.9815386;
z=13;*)
(*Tungsten*)
(*rho=19.3;
dels=0.0005;
Am=183.84;
z=74;*)
(*Beryllium*)
(*rho=1.848;
dels=0.04;
Am=9.012182;
z=4;*)
(*Lithium*)
rho = 0.534;
dels = 0.18;
Am = 6.9412;
z = 3;
(*Boron*)
(*rho=2.46;
dels=0.025;
Am=10.811;
z=5;*)

NA = 6.022141793*10^23;
A = 0.204;
(*160 MeV*)
sigpp = 250.4*10^-27;
signp = 703.26*10^-27;
L = 7*dels;
```

```
(*1.4 GeV*)
(*sigpp=44.4*10^-27;
signp=38.263*10^-27;
L=214*dels;*)
nn = Am - z;
sigma = (sigpp*z + signp*nn)/Am;
Evs = sigma*2*10^13*rho*NA*A*L*0.75^(2/3)*(Pi/Am)^(1/3)
```

Appendix 5: Beam Size Measurements

Measurements were done on the PSB mainly for the purpose of checking how extra coils on some magnets affected the emittance. The cycles used were an LHC type beam and a brighter CNGS type beam. This also resulted in a measurement of the vertical size of the beam. Rather than taking averages, the second smallest of the CNGS beam sizes was used as the worst case scenario involves a narrow CNGS-like beam, but the smallest measurement could be an outlier.

Fit (S): Spline fit, joins the data points

Fit (G): Gaussian approximation

horiz em: Horizontal emittence (similar for vertical)

ep2sig: An estimate of the two sigma emittence

Ring/cycle	Fit	horiz em (mm mrad)	horiz size (mm)	ep2sig (mm mrad)	vert em (mm mrad)	vert size (mm)	ep2sig (mm mrad)	Mean vertical size (mm)
3, LHC	S	10.65	3.92	6.2	4.59	2.57	4.8	2.27
	S	8.16	1.71		4.04	1.21		
	S	3.58	2.27		6.37	3.03		
	G	11.11	4	5.55	4.24	2.47	5.01	2.26
	G	7.81	1.68		4.98	1.34		
	G	2.97	2.07		6.18	2.98		
4, LHC	S	9.19	3.64	6.13	6.47	3.05	5.42	2.40
	S	9.37	1.84		4.46	1.27		
	S	3.34	2.19		5.7	2.87		
	G	8.82	3.56	5.19	5.46	2.8	5.1	2.27
	G	8.32	1.73		4.83	1.32		
	G	2.55	1.92		5.06	2.7		
3, CNGS	S	38.6	7.46	19.06	13.1	4.34	14.26	3.78
	S	26.58	3.09		14.45	2.28		
	S	10.31	3.85		15.42	4.71		
	G	46.72	8.2	21.58	14.29	4.54	16.17	4.04
	G	32.1	3.4		16.25	2.42		
	G	11.02	3.98		18.5	5.16		
4, CNGS	S	33.29	6.92	20.29	15.24	4.68	14.09	3.77
	S	29.93	3.28		13.53	2.21		
	S	10.78	3.94		13.64	4.43		
	G	40.8	7.66	24.66	17.38	5.00	16.92	4.13
	G	38.11	3.7		16.29	2.42		
	G	12.61	4.26		17.13	4.97		

Table 9: *The results from the beam size measurements.*

References

[1] CERN press release PR01.11 31.01.2011, "CERN announces LHC to run in 2012" http://press.web.cern.ch/press/PressReleases/Releases2011/PR01.11E.html

[2] http://linac2.home.cern.ch/linac2/sources/source.htm

[3] CERN FAQ, LHC: The Guide (pp 4-5) http://doc.cern.ch//archive/electronic/cern/others/multimedia/brochure/brochure-2006-003-eng.pdf

[4] http://public.web.cern.ch/public/en/research/AccelComplex-en.html

[5] R. Garoby, *Plans for a Superconducting Proton Linac at CERN*, John Adams Institute For Accelerator Science lecture 10th June 2010 http://www.adams-institute.ac.uk/lectures/?scheme=1&id=12

[6] J. Lettry, M. Kronberger, R. Scrivens, E. Chaudet, D. Faircloth, G. Favre, J.-M. Geisser, D. Küchler, S. Mathot, O. Midttun, M. Paoluzzi, C. Schmitzer, and D. Steyaert, *High duty factor plasma generator for CERN's Superconducting Proton Linac*, Review Of Scientific Instruments Volume **81** Issue **2**, February 2010, 02A723

[7] E. Shaposhnikova (CERN), *SPS Upgrade plan and coating requirements*, AEC'09: anti e-cloud coating workshop 2009 (ACCNET) http://indico.cern.ch/getFile.py/access?contribId=1&sessionId=0&resId=3&materialId=slides&confId=62873

[8] K. Schindl, *The Injector Chain for the LHC*, Proceedings of Chamonix **IX**, January 1999

[9] P. D. V van der Stok, *Multiturn Injection into the CERN Proton Synchrotron Booster,* CERN/PS/BR 81 – 21, December 1981.

[10] E. Noah, F. Gerigk, J. Lettry, M. Lindroos, T. Stora, *EURISOL 100 KW Target Stations Operation and Implications for its Proton Driver Beam*, Proceedings of EPAC 2006, Edinburgh, Scotland.

[11] http://www.lhc-closer.es/php/index.php?i=1&s=3&p=5&e=0

[12] http://isolde.web.cern.ch/isolde/default2.php?index=index/facilityindex.htm&main=facility/facility.php

[13] B. Mikulec, M. Chanel, A. Findlay, K. Hanke, D. Quatraro, G. Rumolo, J. Tan, R. Tomas (CERN), *High Intensity Beams from the CERN PS Booster*, Proceedings of PAC09.

[14] M. Kronberger, D. Küchler, J. Lettry, Ø. Midttun, M. O'Neil, M. Paoluzzi, R. Scrivens (CERN), *Commissioning of the new H− source for Linac4*, Review Of Scientific Instruments Volume **81** Issue **2**, February 2010, 02A708

[15] R. Keller (Los Alamos National Laboratory), *High-intensity ion sources for accelerators with emphasis on H^- beam formation and transport,* Review of Scientific Instruments, Volume **81** Issue **2,** February 2010, 02B311

[16] M. Benedikt (CERN), *PS2/PS2+: Basic Considerations*, LUMI06, Valencia http://indico.cern.ch/getFile.py/access?contribId=40&sessionId=3&resId=1&materialId=slides&confId=4777

[17] W. Scandale and F. Zimmermann (CERN), *Scenarios for sLHC and vLHC*, Nuclear Physics **B** - Proceedings Supplements, Proceedings of the Hadron Collider Physics Symposium 2007, Volumes **177-178**, March 2008, pp 207-211

[18] S. Aumon, B. Balhan, W. Bartmann, J. Borburgh, S. Gilardoni, B. Goddard, M. Hourican, L. Sermeus, R. Steerenberg (CERN), *Feasibility of 2GeV Injection Into The CERN PS*, Proceedings of HB2010

[19] H. Grote and W. Herr (CERN), *Nominal and ultimate luminosity performance of the LHC*, LHC Project Note **275**, January 9, 2002

[20] B. Salvant, N. Mounet, C. Zannini (EPFL and CERN), G. Arduini, O. Berrig, F. Caspers, A. Grudiev, E. Métral, G. Rumolo, E. Shaposhnikova, B. Zotter (CERN), M. Migliorati, B. Spataro (INFN/LNF Frascati) *Update of the SPS Impedance Model*, Proceedings of 1st International Particle Accelerator Conference: IPAC'10, Kyoto, Japan, 23-28 May 2010

[21] M. Pivi (SLAC), *Beam-Beam Effects in Future Linear Colliders*, US Particle Accelerator School January 22-26, 2007 in Houston, Texas, slide 56

[22]: J.-P. Delahaye (CERN), *A review of the possible future HEP Accelerator Projects,* CERN colloquium Thursday 30 September 2010
http://indico.cern.ch/conferenceDisplay.py?confId=108316

[23] Christian Carli, private communication.

[24] CERN Accelerator School, *Fifth General Accelerator Course Proceedings, University of Jyväskylä, Finland*, Volume. **I**, (CERN 94-01)

[25] E. Wilson, *An Introduction to Particle Accelerators* (2001), Oxford University Press

[26] Particle Data Group, *July 2010 Particle Physics Booklet*, Elsevier

[27] Wolfram Research, Inc., Mathematica, Version **7.0**, Champaign, IL (2008)

[28] *Review Of Particle Physics July 2008*, Physics Letters **B** (Elsevier), pp 110, 111, 268

[29] Z. Yuan and K. Mukai, *Effect of boron on the surface tension of molten silicon and its temperature coefficient,* Journal of Colloid and Interface Science, Volume **270** Issue **1**, February 2004, pp 140-145

[30] http://www.chemicool.com/elements/boron.html

[31] D. D. L. Chung , *Composite Materials*, 2nd edition (2010), Springer, p283

[32] T. R. Anthony, W. F. Banholzer, J. F. Fleischer, Lanhua Wei, P. K. Kuo, R. L. Thomas, R. W. Pryor, *Thermal conductivity of isotopically enriched ^{12}C diamond,* Physical Review **B** Volume **42** No **2**, 15 July 1990, pp 1104–1111

[33] S.J. Blundell & K.M. Blundell, *Concepts in Thermodynamics*, 2nd edition (2010), Oxford University Press, pp 101, 265, 461

[34] J. E. Turner, *Atoms, Radiation and Radiation Protection*, 3rd revised & enlarged edition (2007), Wiley, p121.

[35] W. R. Leo, *Techniques for nuclear and particle physics experiments : a how-to approach,* 1987 edition, Springer-Verlag, p25

[36] http://proj-cngs.web.cern.ch/proj-cngs/ProjetOverview/projetoverview2002.htm

[37] G. N. Lewis & M. Randall, *Thermodynamics* (1923), McGraw Hill Book Company, p569

[38] D. R. Lide, *Handbook of Chemistry and Physics*, 89th edition (2009), CRC Press, p 5-45

[39] http://pdg.lbl.gov/2010/hadronic-xsections/pp_total.dat

[40] http://pdg.lbl.gov/2010/hadronic-xsections/np_total.dat

[41] Giovanni Murino, private communication.

[42] http://www.monarchserver.com/TableofEmissivity.pdf

[43] http://www.sp3inc.com/diamond.htm

[44] http://www.chemicalelements.com/elements/b.html

[45] Ralph Assmann, private communication